Chapter II

Synthesis, characterization and application of β-cyclodextrin based magnetic nanoadsorbent for simultaneous adsorption of hydrophilic and hydrophobic dyes

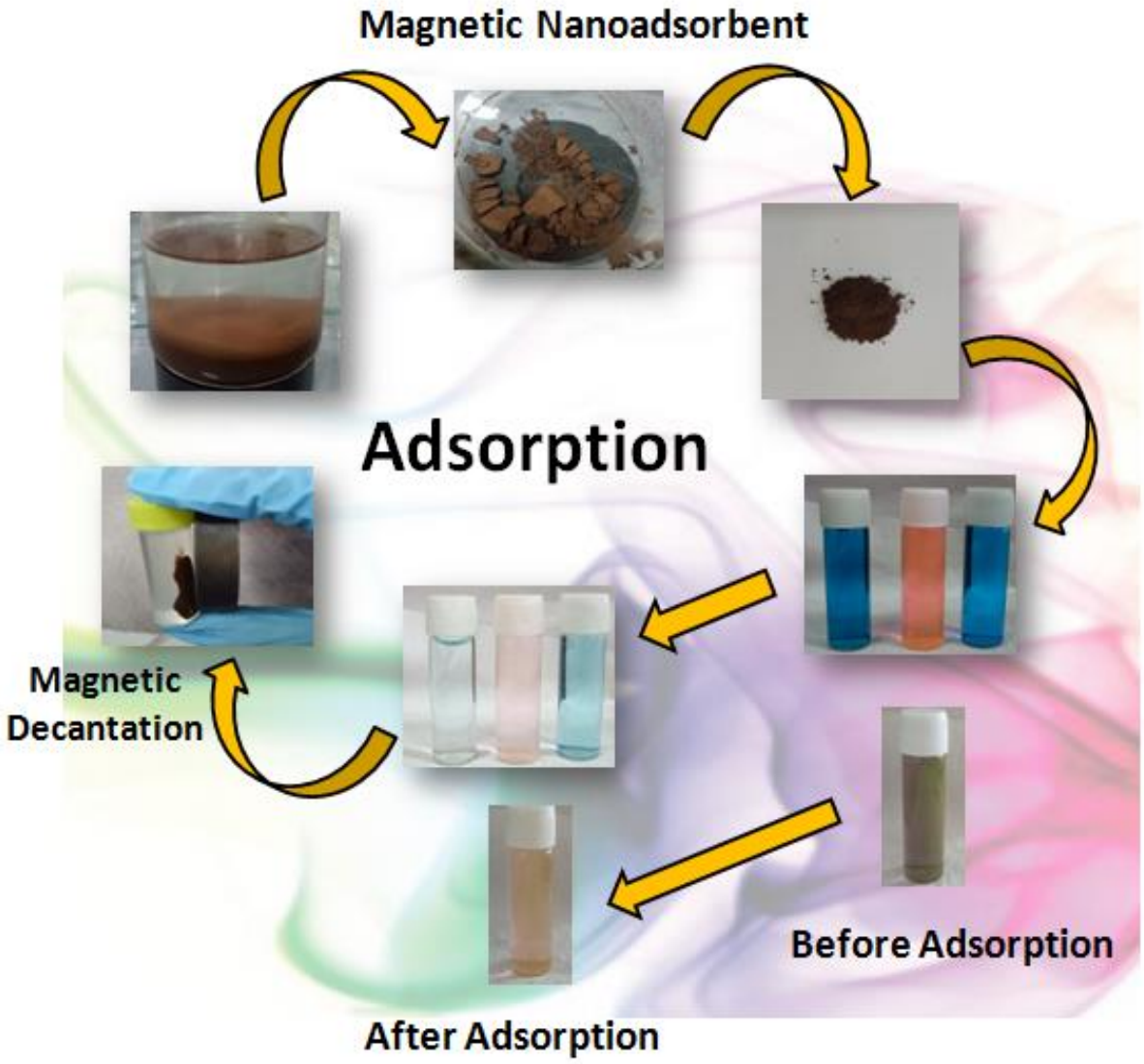

2.1.Introduction

Rising environmental problems due to industrial development in this modern era has gathered more and more attention all over the world. We all are aware of water being a fundamental source of maintaining life on earth. The chemical composition of this abundantly available essential source varies across the strata and also affecting its propriety for domestic and industrial purpose. The effluents of chemical industries such as textiles, paper, color photography, printing, dye and food industries consist huge amount of pollutants such as dyes and paints that poses risk to agriculture and food chain and ultimately to human health. Independent of source, several degradable and non-degradable pollutants are being discharged into the eco-system especially water [1–6]. Dyes are well known colouring agents that transmit colour on final product typically containing higher organic content and colour strength. The complex aromatic molecular structures of synthetic dyes are more resistant towards biodegradation and oxidizing agents. Disposal of such less eco-friendly, unsafe dyes into environment can lead to several disadvantages such as making water odious, causing carcinogenic and mutagenic changes and also hinder light penetration influencing photosynthetic activity. This ultimately leads to increase in chemical oxygen demand (COD) and biological oxygen demand (BOD) of water system[7–9].Therefore, treatment of dye wastewater prior to discharge into water resources of environment is a critical task[10].

Commercially beneficial dyes such as Methylene blue (MB), Malachite green (MG) and Rhodamine are broadly used for dyeing textile fibers like cotton, wools etc. These dyes are also utilized as analytical reagents thus having varied industrial and scientific applications. MB is also utilized for temporary coloring of hairs, although not strongly hazardous, it still has some adverse effects on being consumed such as burning sensations, shock, cyanosis, jaundice, vomiting, difficult inhalation etc.[11]. The triphenylmethane group based cationic dye, Malachite green (MG) is normally indestructible. It is generally used as antibacterial, antiseptic and antiprotozoan agent but oral congestion would be carcinogenic; harmful effects of MG includes excess sweating, fast breathing, respiratory toxicity, teratogenesis, eye burn etc.[12,13] Rhodamine is a relatively hydrophobic, monocationic xanthenes dye generally used as a colorant for food stuffs and textiles as well as dying and tracing agent. Its adverse effects could be neurotoxic, carcinogenic as well as cause chronic and reproductive toxicity in humans and other animals[14]. Several physical, chemical and biological methods have been manifested to eliminate dyes from

wastewater. These include adsorption, electrocoagulation, ozonation, irradiation, ion exchange, membrane and oxidative processes and several others. Among all above mentioned methods, adsorption is considered as one of the most convenient and effective technique for elimination of dyes and effluent treatment.[15] Till date various adsorbents have been developed in order to remove dyes from aqueous solutions. Some of the examples are activated carbon[16], graphene oxide[17], chitosan[18], MCM-41 and MCA[19], polymer-clay[20], mesoporousSiO_2[21], agricultural wastes[22], magnetic bioadsorbent[23], alumina[24], bio-adsorbents, nanoadsorbent [25–27], aerogels[27,28], zeolites[28] and hydrogels[29,30]. The adsorbents having higher removal rate and adsorption capacity are of prime interest for developing effective adsorption system[31]. Due to higher surface area, and ability of surface modification, nanoadsorbents shows greater efficiency and higher removal rate of contaminants from wastewater [26],[32].

Magnetic nanoparticles (MNPs) such as Fe_3O_4 are useful in environmental remediation applications due to rapid dissociation of target molecules from the samples easily by applying an external magnetic field[33],[34]. Magnetic nanoparticles are anticipated to be an efficient heavy metal adsorbent because of its high surface area as well as magnetic recoverability that overcomes the instinctive difficulties of nanoadsorbents to separate from wastewater after use. The coating and modifying magnetic nanoparticles with functional shells are very effective methods to reduce their agglomeration in wastewater and enhancing their adsorption affinity for heavy metals. The amino groups, carboxyl groups and thiol groups are some of the normally utilized functional groups, but mostly papers only report the adsorption properties of nanoadsorbents either with sole amino groups or with sole thiol groups. Magnetic nanoparticles are usually synthesized through crosslinking. Magnetites (Fe_3O_4) are widely used as magnetic cores and numerous methods have been developed for Fe_3O_4 nanoparticles. The easy reflux condition could be used for the synthesis of magnetic nanoparticles with simultaneous surface functionalization using modifiers consisting of functional groups (amine, hydroxyl group and carboxylic). Cyclodextrin (CD), a cyclic oligosaccharides composed of 6 to 8 glucose units, is commonly used as water-soluble functional units to construct polymeric materials through various approaches. CD and its derivatives contains a relatively hydrophobic cavity, hence, it may be used as the molecular recognizer through host-guest interactions[35],[36]. A group of significant contaminants such as polycyclic aromatic hydrocarbons (PAHs), phthalic acid esters (PAEs) and phenolic compounds may consist of inclusion complexes with cyclodextrin and its derivatives. On the basis of these

properties, the cyclodextrin polymer functionalized magnetic nanomaterials have been extensively explored to adsorb and eliminate contaminants from wastewater effectively, which improve the inclusion properties of β-CD and allow for the exploitation of magnetic separation technology of MNPs. Cyclodextrin has host-guest interaction, hydrophobic interaction, or hydrogen-binding interaction and is widely used in drug administration, molecular recognition, supramolecular self-assembly, or catalysis. It interacts with certain environmental contaminants, such as aromatic molecules or heavy metals. As a result, β-cyclodextrin can be utilized in the cleanup of environmental pollutants[37].

Other than this, there are only few reports, regarding logical approach of simultaneous adsorption of multiple dyes. In this study, we have established a facile approach to synthesize magnetic nanoadsorbent for rapid and effective elimination of noxious pollutants such as dyes within few minutes to hours of application.

In the past, we have chemically conjugated MNPs with β-cyclodextrin (CD) using isocyanate linkages [38,39]. The resulting nanoconjugates were capable of successfully encapsulating hydrophobic drug and hydrophilic drug[40]. Inspired by these results we attempted to develop magnetic nanoadsorbent conjugated with cyclodextrin polymer, for simultaneous removal of hydrophobic as well as hydrophilic dyes. Therefore, β-CD based polymers have been utilized for removal of disperse and reactive dyes from aqueous solution[41].

In this study, a super paramagnetic nanoadsorbent (SPNA), was synthesized via covalent conjugation of MNPs with crosslinked cyclodextrin-maleic anhydride copolymer. The efficiency of SPNA as an adsorbent for hydrophobic as well as hydrophilic dyes was assessed under varying concentrations, time and pH. The sorption kinetics and probable mechanism of the adsorption were determined and the data were fitted into various isotherm models.

2.2.Materials and Methods

2.2.1. Materials

β–Cyclodextrin (≥ 97% purity), Maleic Anhydride, Iron Oxide (Fe_3O_4) nanoparticles (97 % purity) and Acetone were purchased from Sigma Aldrich, India. N, N Dimethylformamide (DMF) was purchased from Qualigens, Bombay, India. Methylene Blue (MB), Malachite Green (MG) and Rhodamine-6-G (R6G) were obtained from Fisher Scientific, Navi Mumbai, Laboratory Sulab Reagent, Baroda, and Loba Chemie Laboratory Reagents and Fine Chemicals,

Mumbai, India. Analytical grade reagents were used as received. The solutions of dye were prepared using de-ionized water.

2.2.2. Synthesis of Super paramagnetic Nano-Adsorbent (SPNA)

For the synthesis CD (500 mg) was dissolved in DMF (25 mL), and then solid NaH (15 mg) was slowly added into the solution with vigorous stirring. Further the stirring was continued at room temperature for 6 h. Then solid MA (50 mg) was slowly added to the solution of formed β-CD oxoanion. The reaction mixture was continuously stirred in a sealed round bottom flask in an oil bath at a controlled temperature (100 °C) for 1 h. To this mixture DCC (50 mg) and DMAP (5 mg) were added. 50 mg of Iron Oxide nanoparticles were dispersed in 10 mL of DMF and this dispersion was added to the above reaction mixture. The reaction was stirred for 24 h. The product was precipitated in acetone.

2.2.3. Characterization of SPNA

The NMR spectrum for CD-MA polymer was recorded on Bruker Avance III (400 MHz) NMR spectrophotometer using D_2O as the solvent. PerkinElmer IR spectrophotometer was used to record FTIR spectra of SPNA as KBr discs at room temperature. X-Ray diffractogram were recorded on D2 Phase 2 Bruker X-Ray Powder Diffractometer at room temperature. Vibrating sample magnetometer (VSM) analysis of SPNA was performed by using Lakeshore VSM 7410 at room temperature. In order to accomplish High-Resolution Transmission Electron Microscopy (HR-TEM) analysis Jeol (Jem-2100) electron microscope was used at an acceleration voltage of 200 kV. Dynamic Light Scattering measurements were carried out on Beckman Coulter Delso Nano. Energy dispersive X-ray (EDX) analysis of the vacuum dried SPNA was recorded by the model-JSM-5610 LV. The Surface area and porosity of SPNA were measured using a volumetric adsorption system (Micromeritics Instrument corporation, USA, model ASAP 2020) using N_2 adsorption/desorption isotherms at 77 K up to 1 bar. Before measurements, the samples were activated (degassed) by heating at the rate of 1 K min^{-1} up to 295 K under vacuum. The surface area was calculated using the Brunauer– Emmet–Teller (BET) method and the porosity by the Barrett– Joyner–Halenda (BJH) method. Thermo gravimetric analysis (TGA) was performed using TG–DTA 6300 INCARP EXSTAR 6000 at a heating rate of 10°C/min in the temperature range of 30–500°C with nitrogen atmosphere maintained throughout the measurement.

2.2.4. Adsorption of Dyes

To evaluate the adsorption capacity of SPNA, two hydrophilic dyes, Methylene Blue (MB), and Malachite Green (MG) and a hydrophobic dye, Rhodamine-6-G (R6G) were used as model dyes for adsorption studies. The adsorption process was carried out in 100 mL conical flasks containing 10 mL of dye solutions. To determine the optimum quantity of SPNA to be used in subsequent experiments, different amounts (10, 15 and 20 mg) of SPNA was added in 50 mg/L of prepared dye solutions individually. All the solutions were placed on magnetic stirring for different time intervals, aliquots were collected and further measured for content of un-adsorbed dye using UV-Vis Spectrophotometer. For determining optimum concentration of dyes to be used in successive experiments, different concentrations (10 – 50 mg/L) of dyes were prepared and optimum amount of SPNA was added to the solutions. All the solutions were placed on shaker for 24 h at 27°C and shaking speed of 160 rpm to attain equilibrium condition. Supernatant was separated by applying external magnetic field and analyzed using UV-visible spectrophotometer at the wavelength range of 400-800 nm. To determine optimum pH for adsorption, 10 mL of 30 mg/L MB, MG and R6G were taken with 50mg SPNA at different pH and kept on shaker for equilibrium study, supernatants were collected after adsorption and analyzed using Jasco V-730 UV-Visible Spectrophotometer (λ_{max} = 664 for MB, λ_{max} = 617 for MG and λ_{max} = 526 for R6G).The adsorption capacity, removal percentage and adsorption at particular time‘t’ were calculated using the following equations[10]:

$$q_e = \frac{(C_0 - C_e)}{m} * V \ldots\ldots\ldots\ldots\ldots (1)$$

$$\%R_e = \frac{C_0 - C_e}{C_e} * 100 \ldots\ldots\ldots\ldots (2)$$

$$q_t = \frac{C_0 - C_t}{m} * V \ldots\ldots\ldots\ldots\ldots (3)$$

where,

q_e denoteadsorption capacity (mg/g), q_t is adsorption capacity at particular time ‘*t*’ (mg/g) and *%Re* is the removal percentage of dyes; C_0 represents initial concentration (mg/L), C_e is equilibrium concentration (mg/L) and C_t denote the concentration at time ‘*t*’ (mg/L) of dyes in

aqueous solution; '*V*' denotes the volume of solution (L) and '*m*' denotes the weight of the adsorbent (g).

2.2.5. Simultaneous Adsorption Studies of Hydrophilic and Hydrophobic Dyes

Since the adsorbent was able to adsorb hydrophilic dyes with greater efficiency it was interesting to investigate the simultaneous adsorption of Hydrophilic and Hydrophobic Dyes in binary mixture. For this purpose, binary system of MG-R6G having an initial concentration of 30 mg/L, pH 7.0 and was used. To ensure that both the dyes reach an equilibrium time of 24 h was selected for these binary experiments.

2.2.6. Desorption Experiment and Reusability

SPNA (20 mg) was placed in conical flask containing 50 mg/L dye solutions individually and solutions were magnetically stirred for 5 hours. Dye solutions were separated using external magnetic field and final concentrations of dyes were determined. The SPNA was desorbed by washing it under constant stirring with 1:1 ethanol and water for three times respectively, dried and stored to start new adsorption batch [42].

2.3.Results and Discussion

2.3.1. Synthesis of SPNA

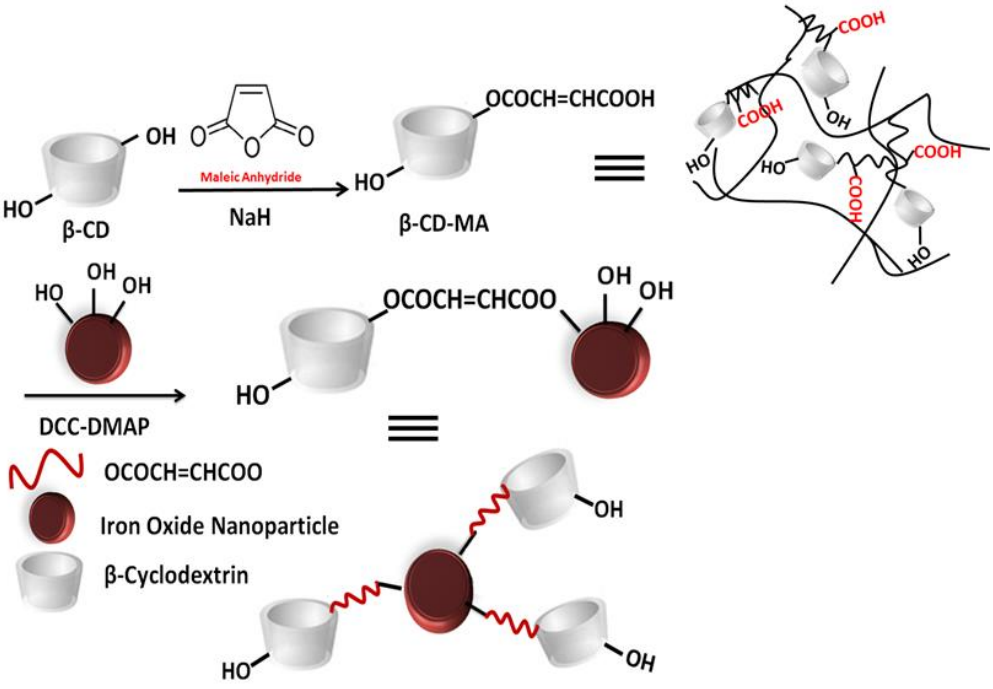

Figure 2.1: Schematic for synthesis of SPNA

The superparamagnetic nano-adsorbent was synthesized according to the schematic shown in **Figure 2.1**.Crosslinking of CD with maleic anhydride leads to decrease in its solubility making it more suitable as an adsorbent. The cyclodextrin polymer (CD-MA) is synthesized by crosslinking cyclodextrin with maleic anhydride via oxoanion intermediate by nucleophilic substitution reaction. The oxoanion is formed due to the generation of strong alkaline conditions by addition of NaH which causes deprotonation of the hydroxyl group at C2 position of the anhydrous glucose unit. The next step is functionalization of iron oxide nanoparticles with CD-MA. MNPs have hydroxyl groups on their surface which react with the free carboxyl groups of CD-MA via ester linkages to give the final product.

2.3.2. NMR Spectra Analysis

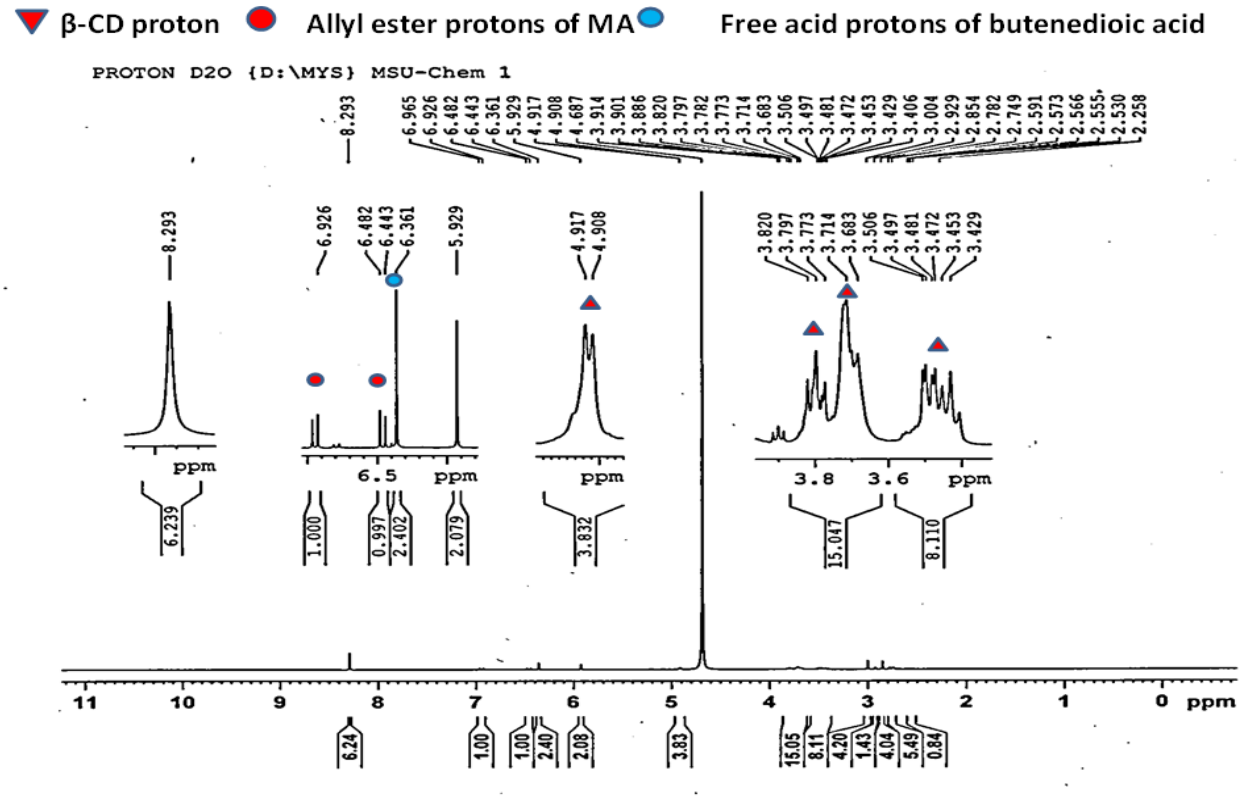

Figure 2.2: NMR spectra for CD-MA

The structure of CD-MA polymer was verified by proton NMR (**Figure 2.2**). The spectra shows characteristic peaks of protons for free acids at 6.36 ppm. The vinylic protons of Maleic monoesters were observed at 6.46 and 6.92 ppm. The protons of β-Cyclodextrin from repetitive unit of glucose appear at 4.91 ppm for H1, 3.50 ppm for H2, 3.68-3.82 ppm for H3, H5, H6 and

3.43-3.47 ppm for H4[43]. The NMR spectra of maleic anhydride and CD are represented in **Figure 2.3** and **Figure 2.4** respectively.

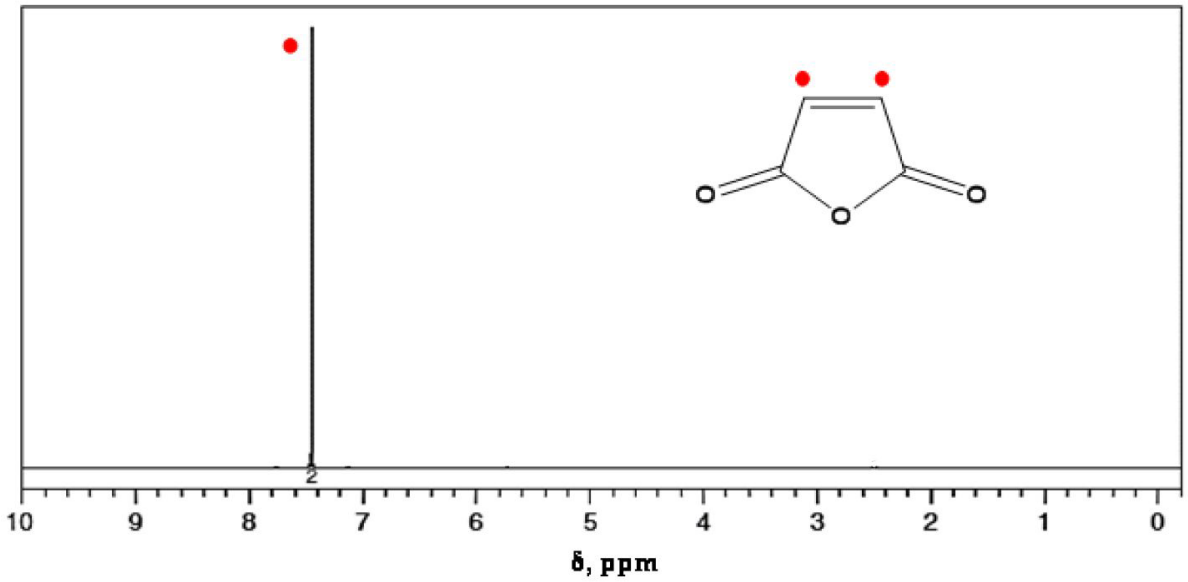

Figure 2.3: 1H NMR spectra of Maleic Anhydride

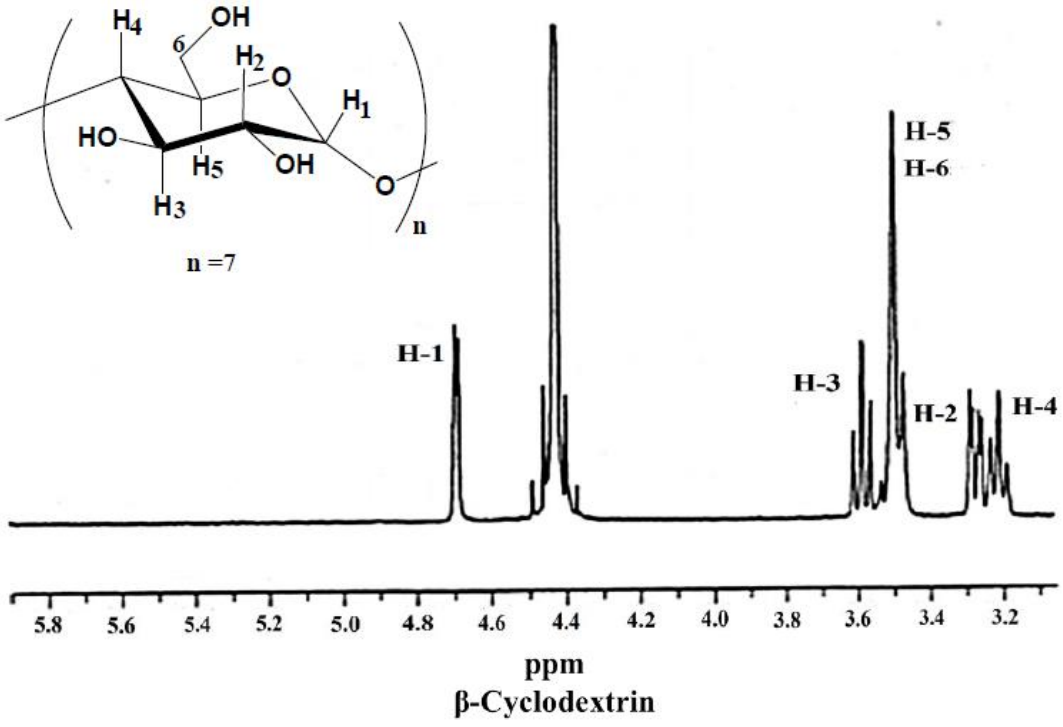

Figure 2.4: 1H NMR spectra of β- cyclodextrin polymer

2.3.3. FTIR Spectra Analysis

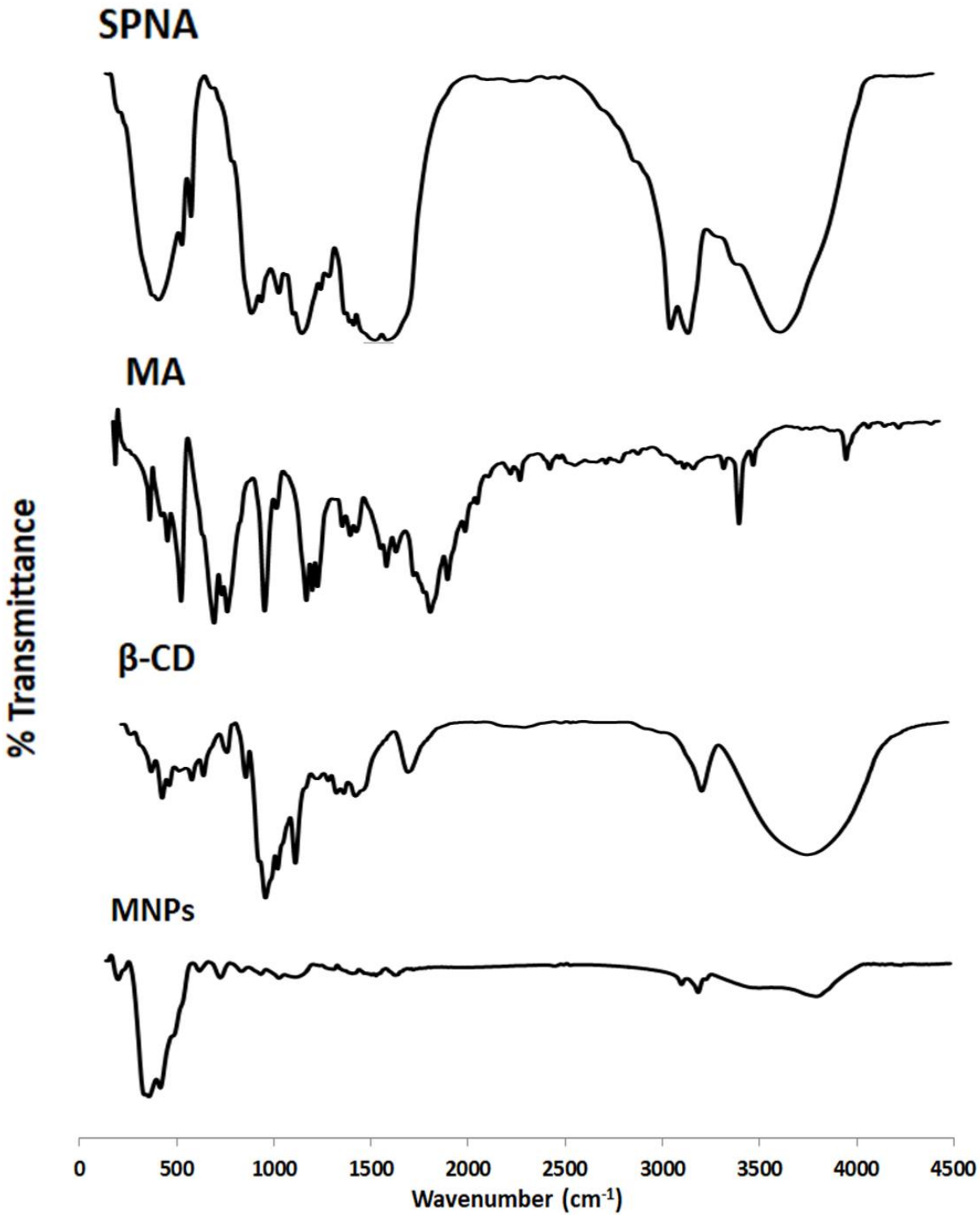

Figure 2.5: FTIR spectra of MNPs, β-CD, MA, and SPNA

The IR spectra of β-cyclodextrin shows a characteristic broad band within the range of 3300–3500 cm^{-1} which corresponds to the presence of hydroxyl groups (**Figure 2.5**). The IR spectra for SPNA also shows a broad band at 3461–3173 cm^{-1}due to –OH stretching vibrations which corresponds to the incorporation of cyclodextrin moieties on SPNA. The absorption band at 1854 cm^{-1} corresponding to carbonyl stretching frequencies is observed in the spectra for maleic anhydride. However in the spectra of SPNA the C=O stretching frequency is observed at 1725 cm^{-1} the shift is corresponding to the formation of ester linkages. Moreover the absorption band at 2829.6 cm^{-1} corresponds to asymmetric C–H stretching vibration further confirms that ester bond is formed. The peak at 1589 cm^{-1}signifies the presence of C=C in maleic anhydride the same peak is observed at 1574 cm^{-1} thus proving the attachment of maleic anhydride unit. The peaks at 1023 and 1152 cm^{-1} corresponds to the antisymmetric (C–O–C) vibrations and coupled (C–C/C–O) stretching vibration. The peak observed at 772 cm^{-1} in the spectra of both MNPs and SPNA indicates successful conjugation of the polymer on the surface of iron oxide nanoparticles.

2.3.4. X-Ray Diffractogram Analysis

The XRD diffractogram of SPNA (**Figure 2.6**) showed exhibited peaks at 30.30, 35.56, 56.68 and 62.75 corresponding to (220), (311), (511) and (440) planes of Fe_3O_4, respectively. This leads to a conclusion that the incorporation of polymer does not change the crystal phase of MNPs[44].

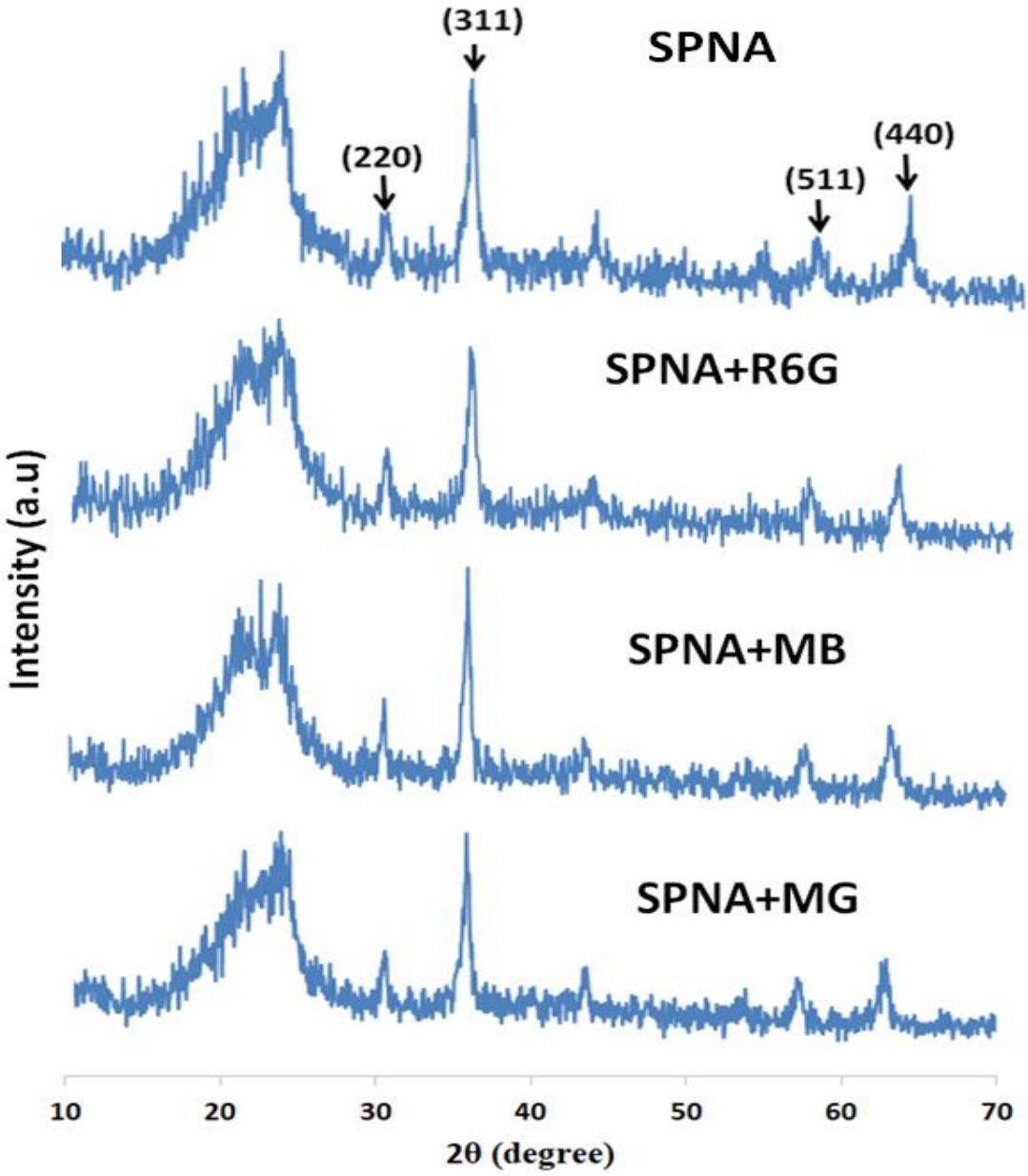

Figure 2.6: XRD pattern for fresh SPNA and recycled SPNA

2.3.5. HR-TEM Analysis

The HR-TEM images (**Figure 2.7**) represent the size distribution of MNPs and SPNA. Pure MNPs were observed as nano-sized aggregates having a size range of 20-30 nm. However SPNA appeared as spherical and discrete monodispersed particles having narrow size distribution of 50-60 nm. This suggests that the thickness of CD-MA polymer on MNPs is approximately 20-30 nm. Moreover image C shows a distinct layer of light field contrast which arises due to the

polymer coating on the surface of the iron oxide nanoparticles. This also provides an evidence for the successful coating of CD-MA on MNPs.

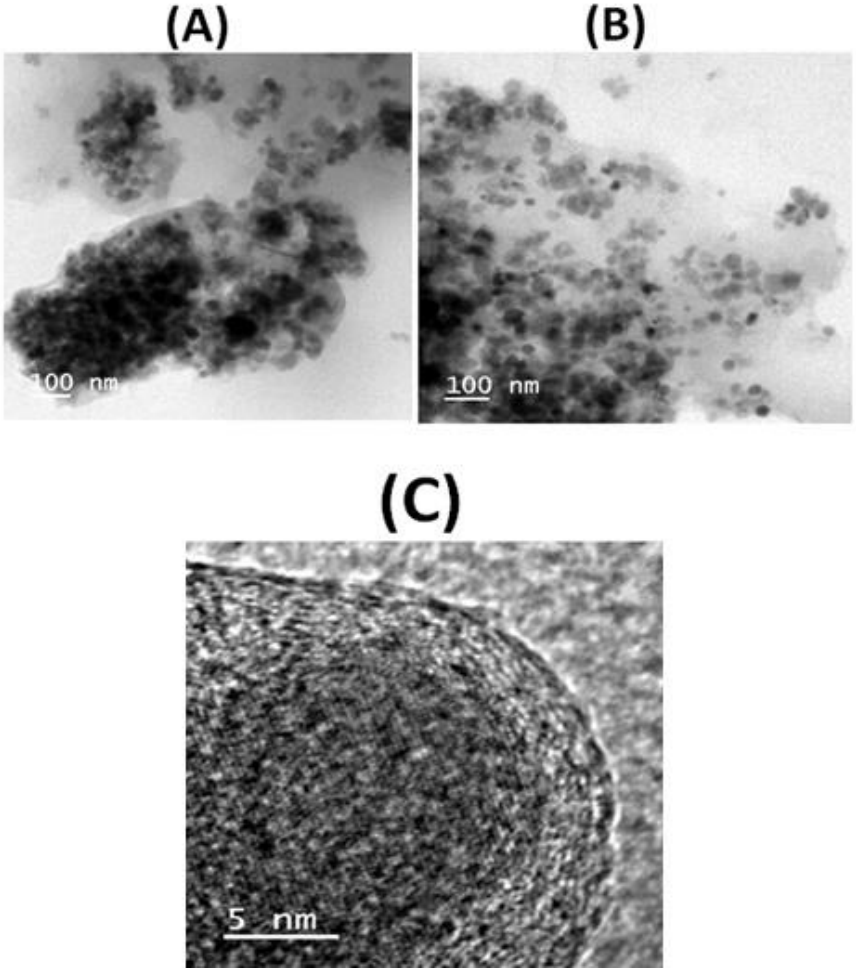

Figure 2.7: HR-TEM images for (A) Pure MNPs and (B) & (C) SPNA

2.3.6. Dynamic Light Scattering Analysis

The hydrodynamic diameter of SPNA was determined using Dynamic Light Scattering experiments. At 25°C, the diameter was observed to be 57 nm moreover the particles were monodispersed which is concordant with the data of HR-TEM (**Figure 2.8**).

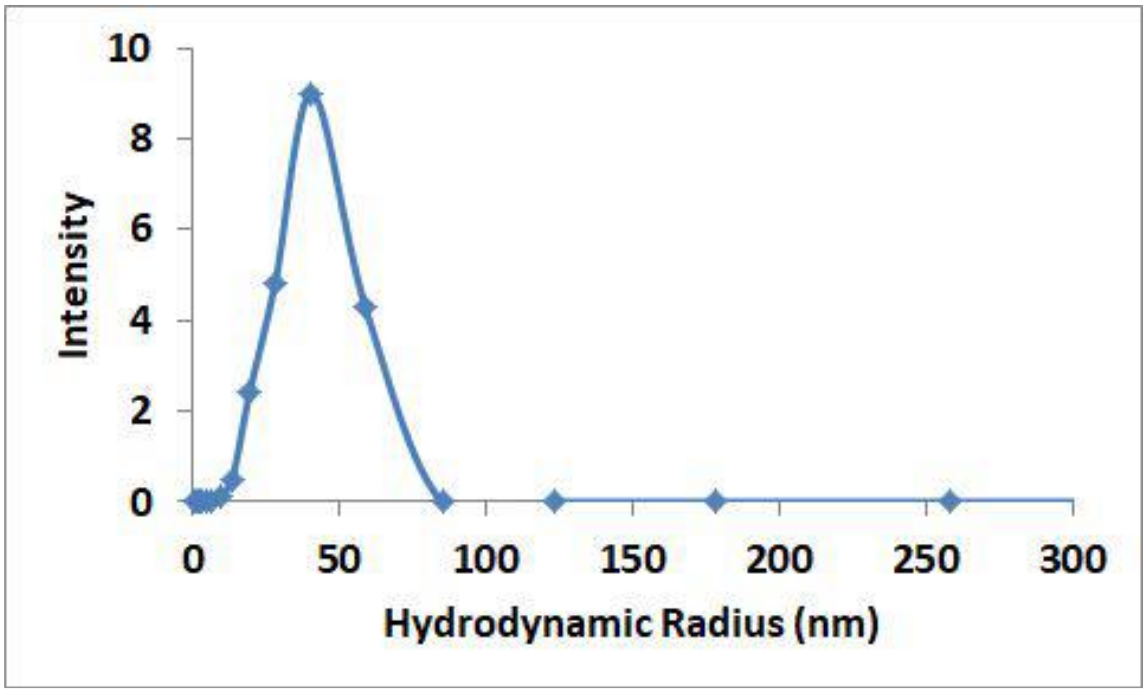

Figure 2.8: DLS profile for SPNA

2.3.7. VSM Analysis

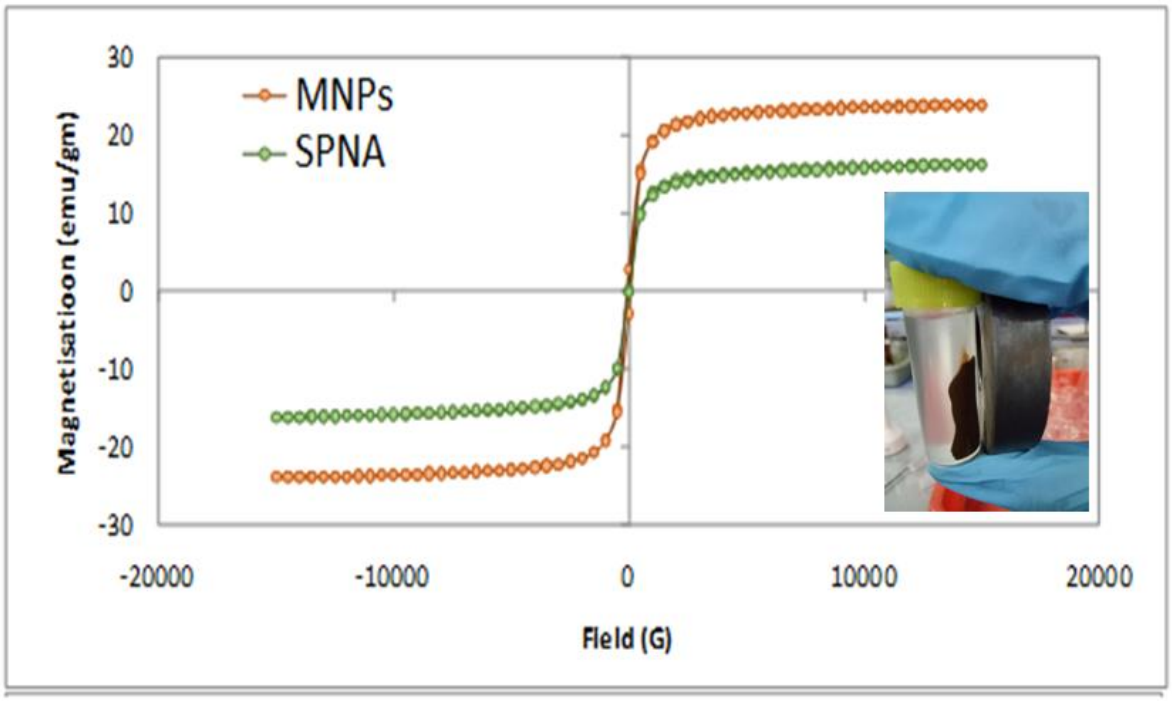

Figure 2.9: Room temperature magnetization curves of SPNA (Inset: Photograph showing separation of SPNA using an external magnet)

The performance of magnetic materials can be assessed by hysteresis loop determinations at ambient temperature using VSM. The VSM measurements of bare MNPs and SPNA are shown in **Figure 2.9**.The magnetic properties are measured as a function of magnetic field, time and temperature. It can be observed from the M-H loops that SPNA shows ferromagnetic behavior. A decrease in the magnetization value was observed in case of SPNA which is due to coating of polymer on MNPs. However, the material could be easily dispersed and withdrawn with the help of an external magnet. This observation suggests that the magnetism of the iron oxide nanoparticles at the core is retained even after conjugation with CD-MA.

2.3.8. TGA Analysis

The nanoadsorbent was analyzed with TGA (**Figure 2.10**) for the assessment of its thermal properties. Three stages of degradation were observed for the adsorbent. A mass loss of 4.5% corresponding to removal of adsorbed water molecules was observed below 200 °C. In the second stage of degradation in a temperature range of 200 °C to 350 °C about 36.8% mass loss is observed attributing to breaking of ester linkages [46]. The final degradation of 11.4% in the 360 °C to 500 °C range occurs as a result of decomposition of CD molecules [47].

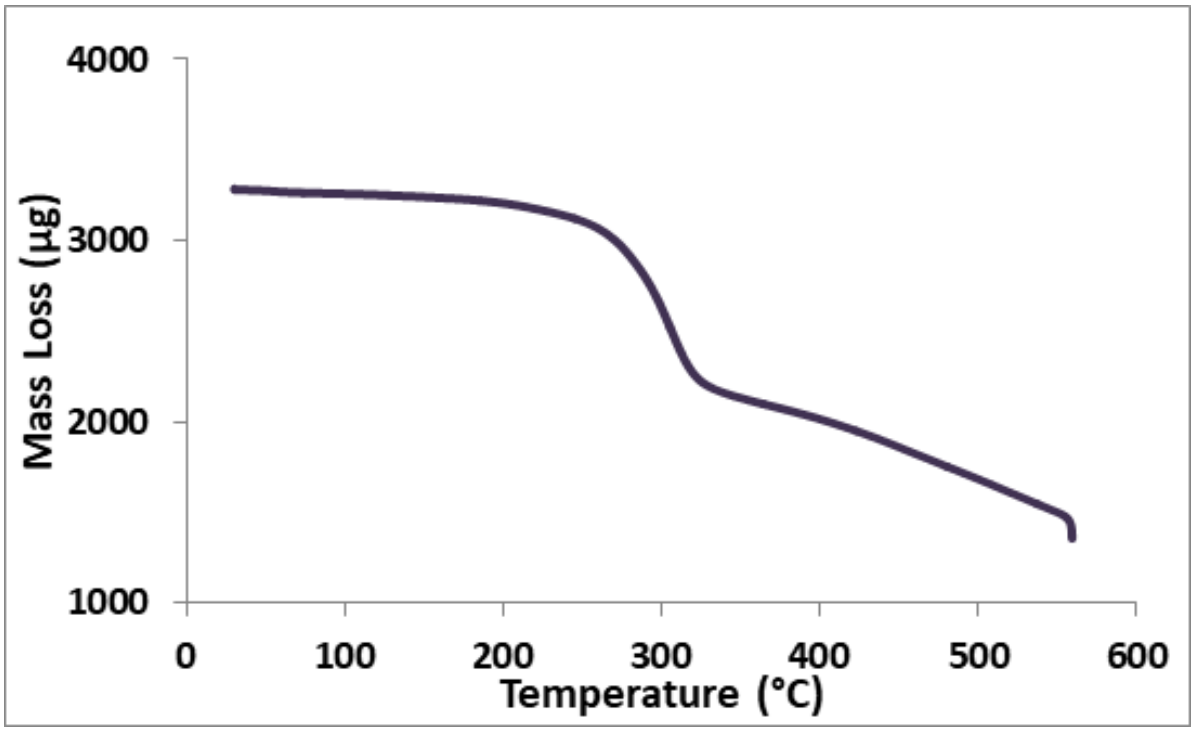

Figure 2.10: Thermo Gravimetric Analysis curve of SPNA

2.3.9. BET Analysis

The BET adsorption isotherm is shown in **Figure 2.11**,exhibits the shape of the type II isotherm as per IUPAC classification, thus suggesting that these particles are mostly non-porous or macro-porous[48]. Thus SPNA has the possibility of showing physisorption or monolayer adsorption[49].The BET specific surface area, total pore volume and average pore diameter of sample is presented in **Table 2.1**. The BET adsorption isotherm of pristine iron oxide nanoparticles is shown in **Figure 2.12**.

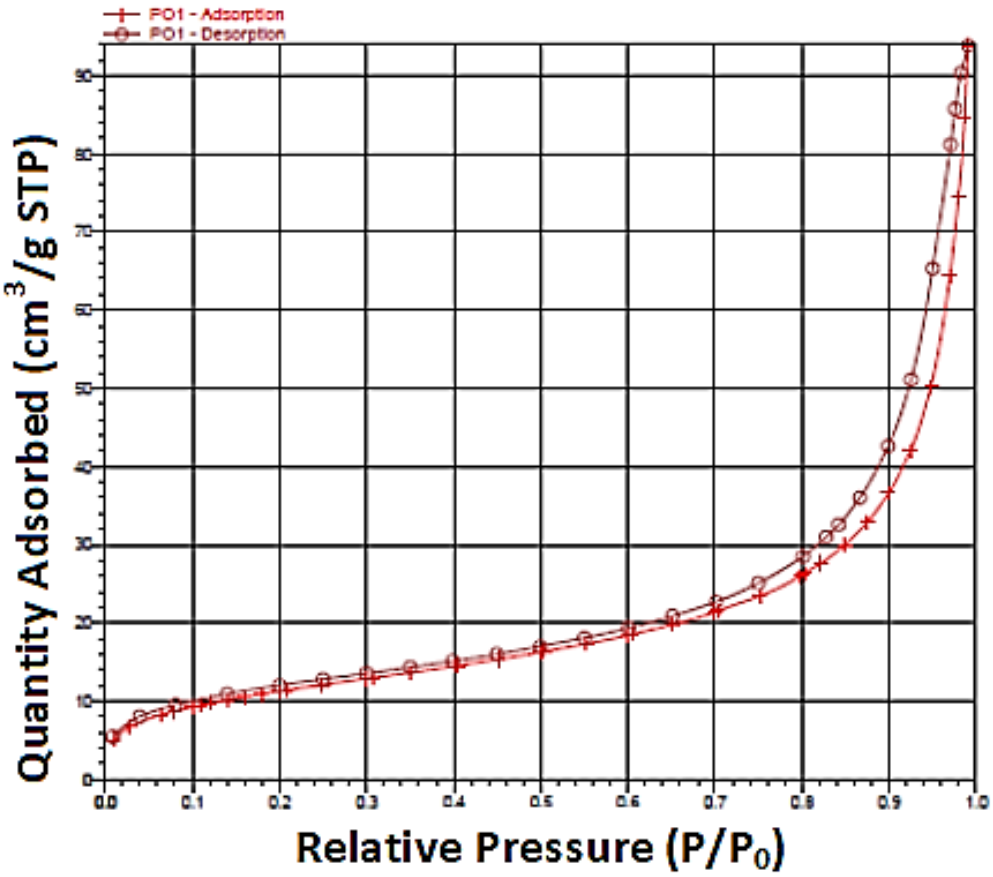

Figure 2.11: Nitrogen adsorption−desorption isotherm of SPNA

Table 2.1: BET Parameters of SPNA

Sample	BET Plot		
SPNA	**Average Pore Diameter (nm)**	**BET specific Surface Area (m^2/g)**	**Total Pore Volume (cm^3/g)**
	14.96	40.7369	0.143870

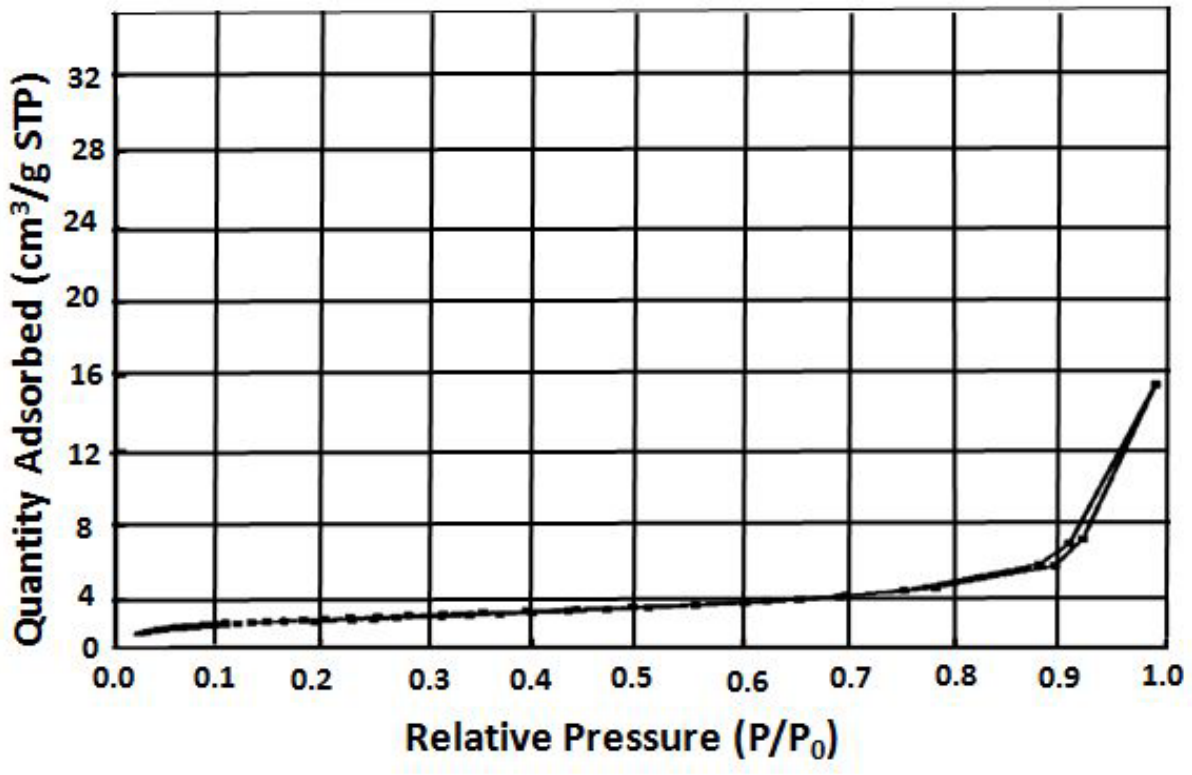

Figure 2.12: Nitrogen adsorption-desorption isotherm of pristine Iron Oxide Nanoparticles (BET Specific Surface Area- 6.8 m2/g, Pore Volume- 0.025 cm3/g)

2.3.10. Selectivity of Adsorption (Effect of Cavity of Cyclodextrin)

The CD-MA polymer facilitates the uptake of hydrophilic as well as hydrophobic dye molecules via various chemical interactions making SPNA a versatile adsorbent. The hydrophobic cavity of cyclodextrin is likely to encapsulate the hydrophobic dye R6G more than the cationic dyes due to which it is expected to get adsorbed to a greater extent. However the results from the adsorption experiments show an interesting trend. The removal of hydrophilic dyes is more than hydrophobic dye. Comparison further shows that removal of MG is the maximum amongst the 3 dyes and removal efficiency for R6G is the least. The higher adsorption efficiency for MG can be attributed to the small spatial prohibition for the structure of MG molecule. This leads to rapid interaction of MG molecules with SPNA. However, although there is availability of the hydrophobic cavity of cyclodextrin for R6G the steric hindrance caused due to large spatial size causes the encapsulation within the cavity difficult and hence less adsorption as compared to MB and MG. Various other factors which lead to this phenomenon have been explained further.

2.3.11. Effect of SPNA dosage

The quantity of adsorbent corresponds to the available active sites and hence plays an important role in the process of adsorption. The effect of SPNA quantity on the percentage removal of the dyes was evaluated at pH 7.0 for 24 hours. The results of this study are shown in **Figure 2.13**. It is observed that the maximum percentage removal was obtained using 20 mg of SPNAs for all the three dyes. The increase in the removal efficiency from 10 mg to 20 mg corresponds to higher availability of active interaction sites due to large surface area with the increase in the quantity of adsorbent. Further increase in dosage causes a decrease in the removal efficiency. This can be explained by two reasons. Firstly, the magnetic property of the adsorbent results in formation of aggregates during the process of adsorption. This causes a decrease in the exposed surface area available for adsorption and thus affecting the removal efficiency. Secondly an increase in the amount of the absorbent causes a decrease in the rate at which the active adsorption sites are utilized by the adsorbate molecules which lowers the percentage removal. Thus, 20 mg is the optimum quantity of the adsorbent.

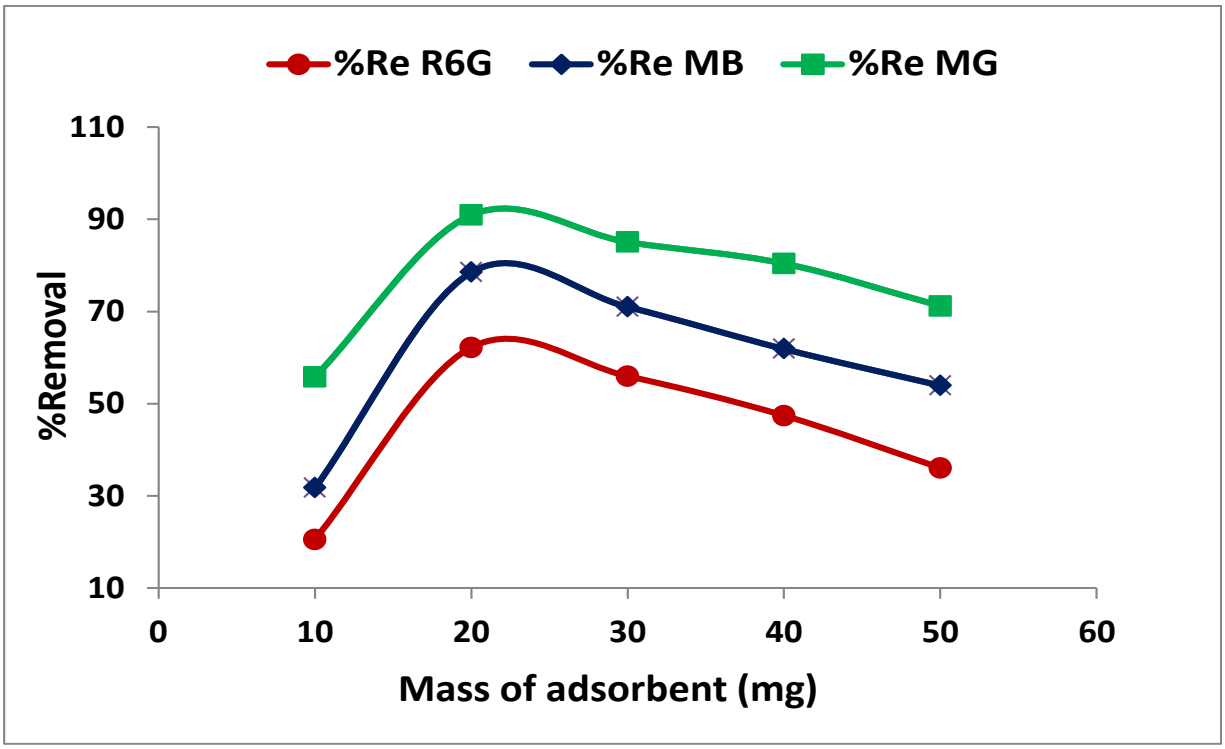

Figure 2.13: Effect of SPNAs dosage on the percentage removal of 30 mgL^{-1} of MG, 20 mgL^{-1} of MB and R6G at 25 °C and pH-7.0.

2.3.12. Effect of contact time

Figure 2.14 shows the effect of contact time on the adsorption of dyes by SPNAs at 5, 10, 15, 20, 25 and 30 minutes (pH 7.0 and 25 °C). It was observed that the equilibrium is attained in 30 minutes. The removal efficiency of the three dyes are different at the end of 30 minutes which is because of difference in interaction of the dyes with the adsorbent. The removal of MG is considerably fast as compared to that of MB and R6G. The process of adsorption can be elaborated in three stages, firstly the dye molecules migrate thorough the solution to reach the adsorbent surface. After this certain dye molecules are adsorbed via Van der Waals force. Electrostatic interactions between the cationic dye and the adsorbent consist of the last stage. As the process of adsorption begins the removal increases with time which corresponds to the attachment via Van der Waals forces and then via electrostatic interactions when the dye is in close proximity of the adsorbent. After lapse of time, the vacant sites cannot be further occupied by the dye molecules. This corresponds to the attainment of equilibrium.

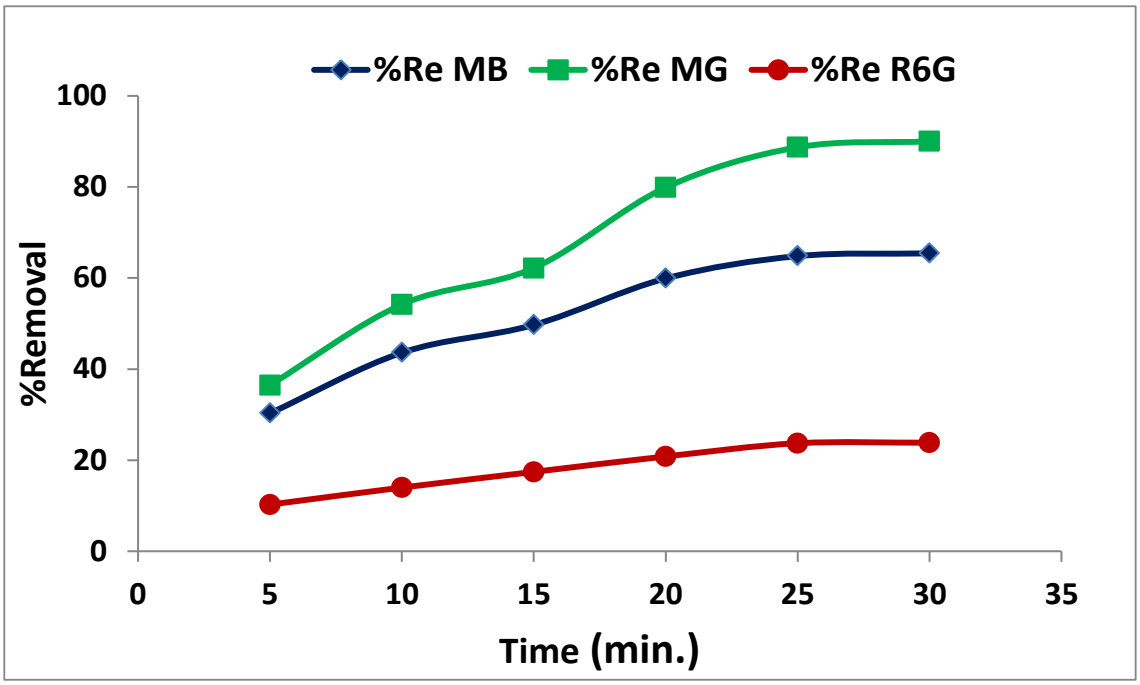

Figure 2.14: Effect of contact time on the percentage removal of 30mgL^{-1} of MG, 20 mgL^{-1} of MB and R6G at 25 °C and pH-7.0

2.3.13. Effect of pH

The pH of the solution plays an important role during the process of dye adsorption. This occurs because pH affects the adsorbent as well as the dye molecules, for instance the surface charge of

the adsorbent, the structure of dye molecules and the extent to which ionization of dyes occur [50].The effect of pH is illustrated in **Figure 2.15**. It was observed that maximum adsorption of the dye is obtained under basic conditions (pH 9). This phenomenon occurs because the cationic nature of Malachite Green and Methylene Blue. The adsorbent possess negatively charged functional groups on their surface that are dissociated at different pH values. Hydroxyl groups hold their protons (OH) in protonated form at pH less than 4.0, due to which interaction between negatively charged groups (O^-) and positively charged dye molecules withers because a competition arises between hydrogen ion in the solution and cationic dyes for active functional sites on the surface of adsorbent. The functional groups deprotonate (O^-) with increasing solution pH, that ultimately results in enhancing negative charge density on the surface of adsorbent that accelerate the binding of adsorbate molecules. Therefore, the main interaction between binding of cationic dye molecules and negatively charged adsorbent surface involved electrostatic interaction, whereas physical adsorption is the mechanism of the process of adsorption on the basis of electrostatic interaction[51].

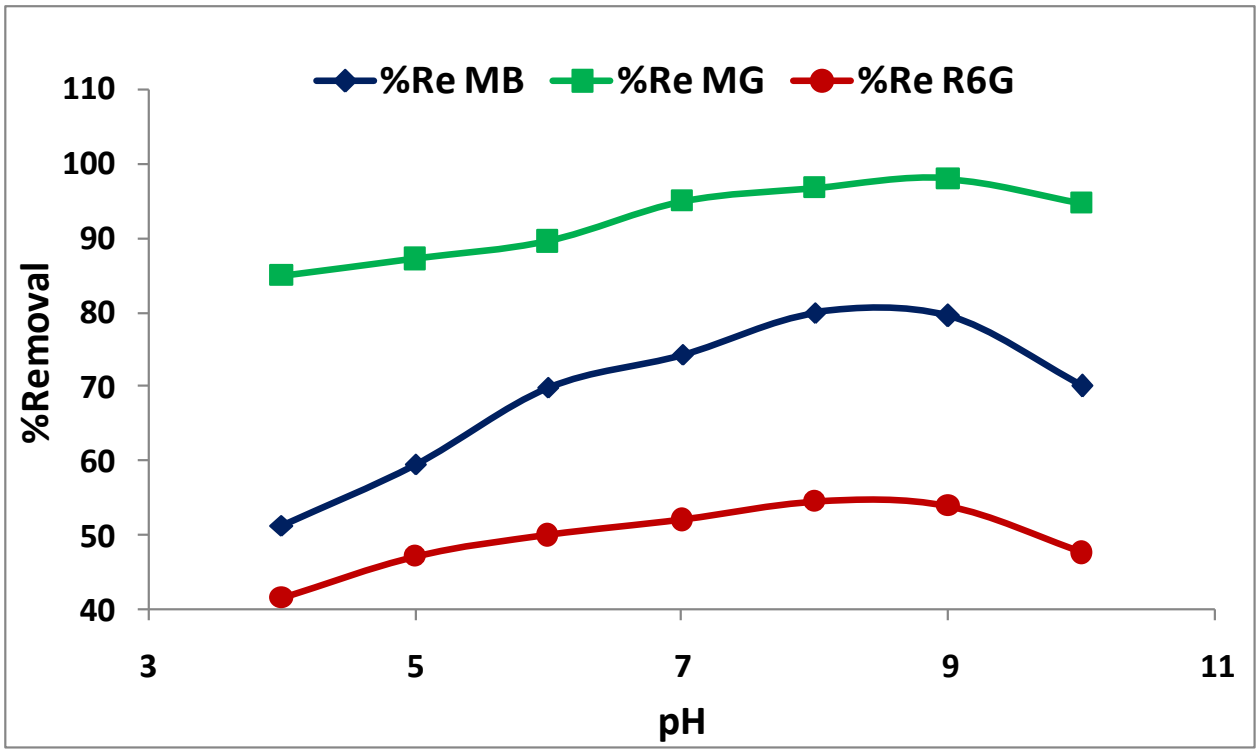

Figure 2.15: Effect of pH on the percentage removal of 30 mgL^{-1} of MG, 20 mgL^{-1} of MB and R6G at 25 °C

2.3.14. Effect of Initial Concentration

The effect of Initial Concentration illustrated in **Figure 2.16** shows that the rate of adsorption increases rapidly before the concentration reaches the maximum 30 mg/L for MG and 20 mg/L for MB and R6G.The rate of adsorption then decreases and becomes constant. This phenomenon occurs because initially due to higher concentration of the dye there is a mass gradient enhancement between the solution and the adsorbent, this is the driving force for the migration of dye molecules from the bulk of the solution to the surface of adsorbent. After attainment of equilibrium the decrease in number of active sites does not favor further adsorption which explains the decrease and further constant nature of the graph. [52]

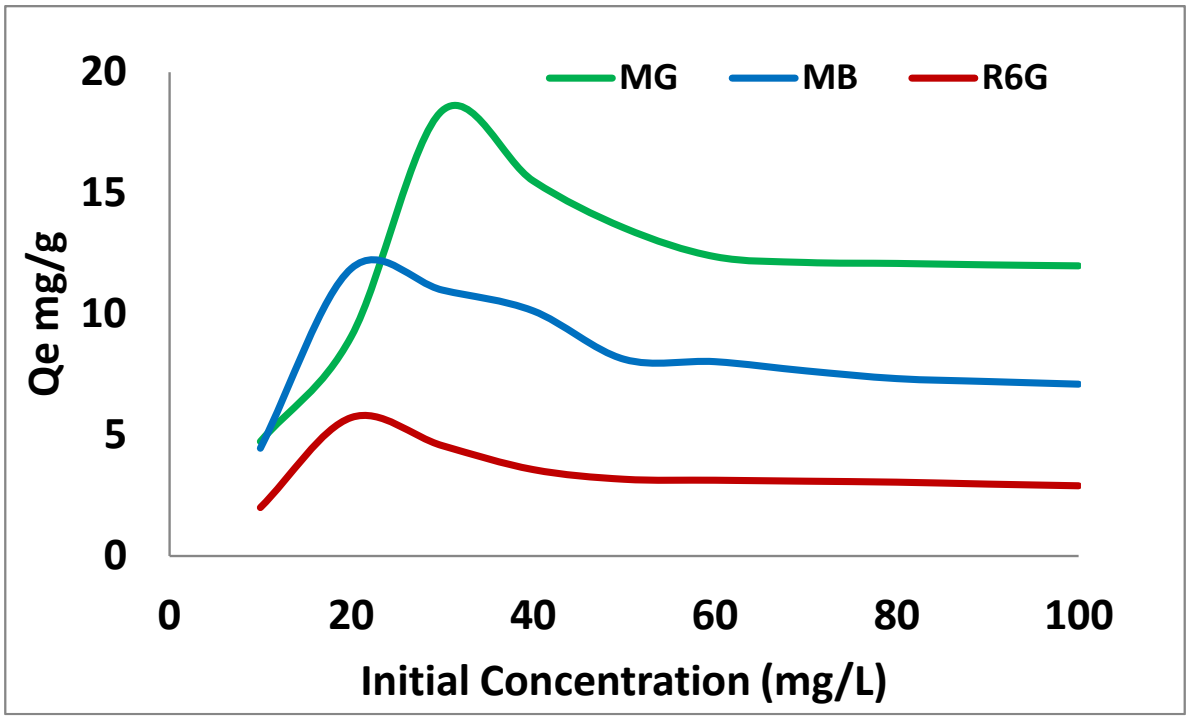

Figure 2.16: Effect of initial concentration on adsorption of dyes on SPNA

2.3.15. Effect of Temperature

The dye removal increases with the increase of temperature. In case of MG, %Re increases from 87.9% to 97.2% by increasing the temperature by 10 °C. Similarly for MB the removal increases from 80.2% to 85.1% and for R6G it is from 30.5% to 37.3% as shown in **Figure 2.17**. An increase in temperature not only enhances the mobility of dye molecules but also provide

sufficient energy which facilitates the interaction between the active sites and dye molecules. This causes an increase in the adsorption of dye at higher temperature.

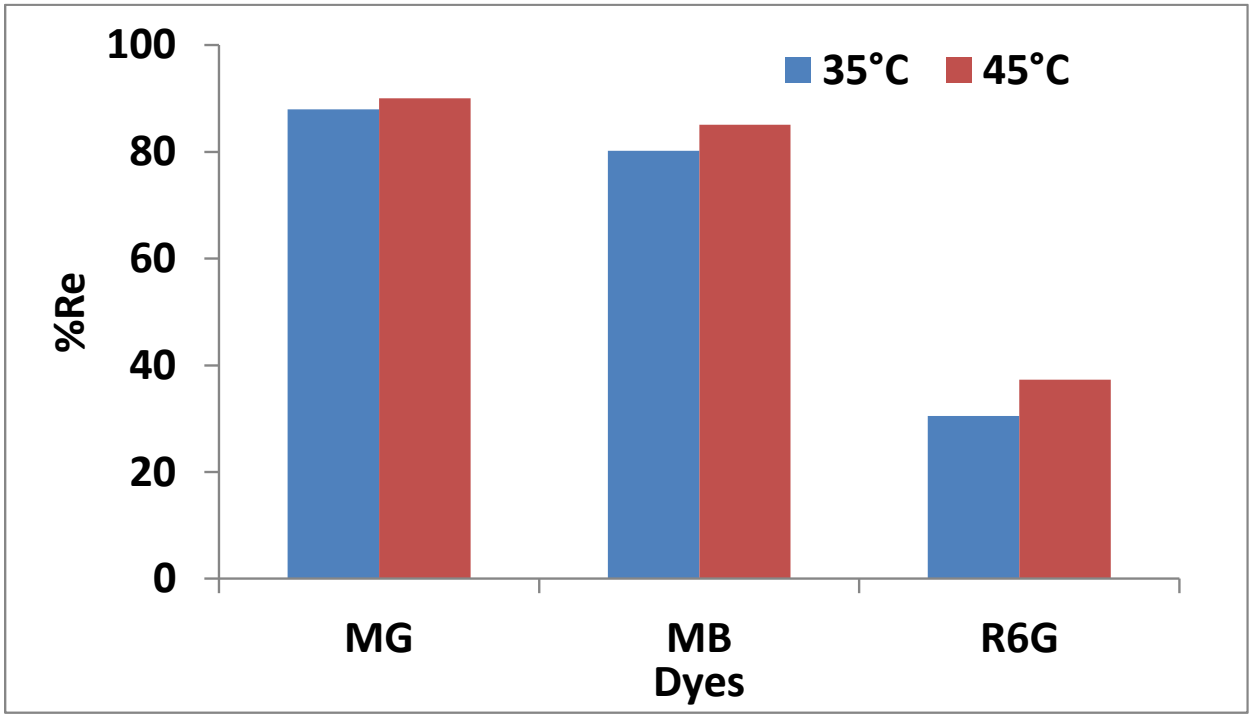

Figure 2.17: Effect of temperature on dye removal efficiency at 35 °C and 45 °C

2.3.16. Adsorption isotherms

The relationship between the adsorption capacity (q_e) and concentration of solution after adsorption at a particular temperature is illustrated using an adsorption isotherm. They are imperative for designing an adsorption system and its data analysis. In this context, adsorption capacities of the dyes onto SPNA were evaluated by Langmuir and Freundlich adsorption isotherm models (**Figure 2.18 and 2.19**).

$$\frac{Ce}{q_e} = \frac{1}{K_L} + \frac{Ce}{q_m} \ldots\ldots\ldots\ldots (4)$$

$$lnq_e = lnK_F + \frac{1}{n} lnCe \ldots\ldots\ldots (5)$$

where, C_e (mg L^{-1}) is the equilibrium concentration of dyes, q_e (mg g^{-1}) is the adsorption capacity of SPNAs at equilibrium; q_m is the maximum adsorption capacity (mg g^{-1}); K_L and K_F (L/mg) are the Langmuir and Freundlich equilibrium adsorption constants.

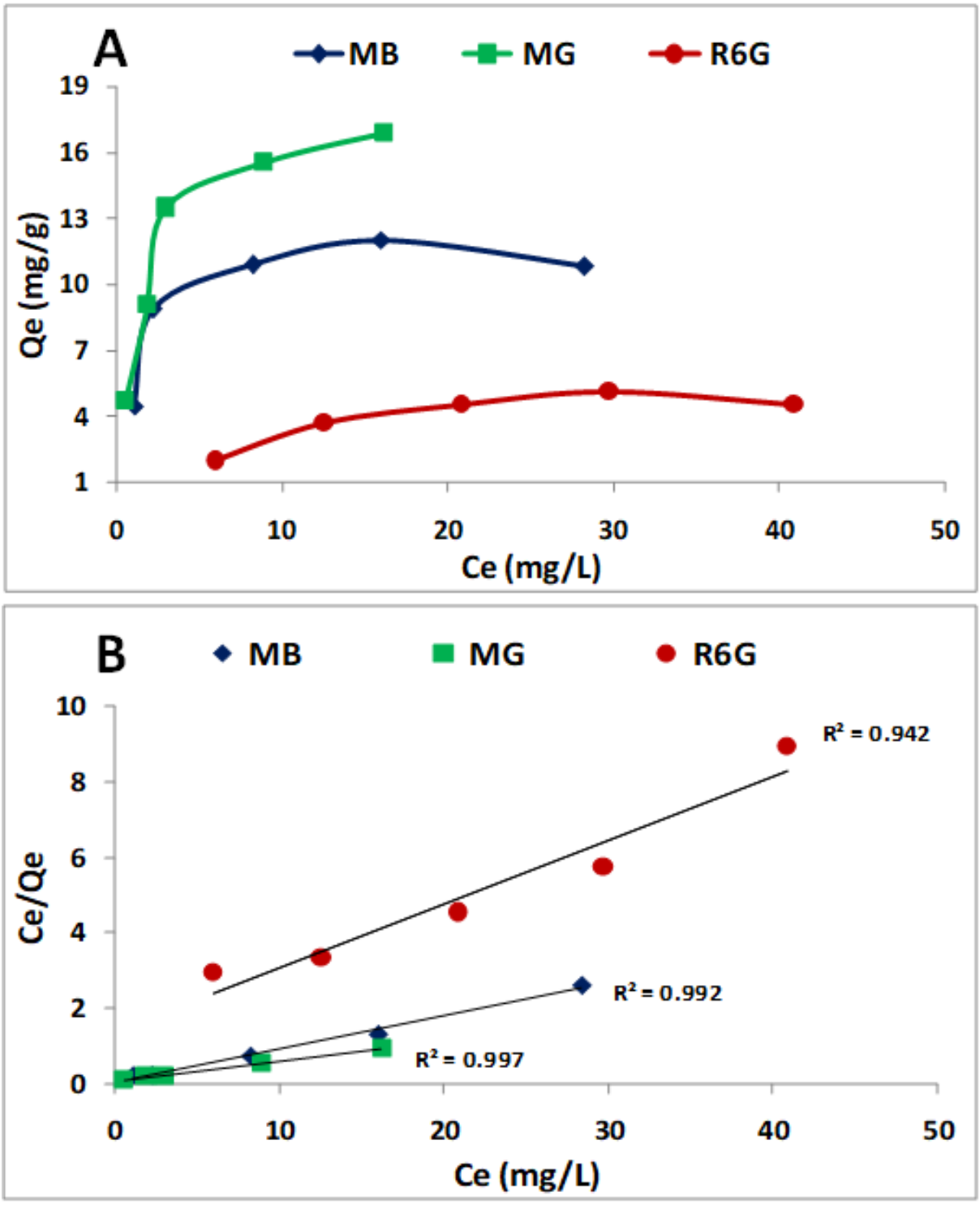

Figure 2.18: Langmuir adsorption isotherm for the removal of 30 mgL^{-1} of MG, 20 mgL^{-1} of MB and R6G at 25 °C pH 7.0

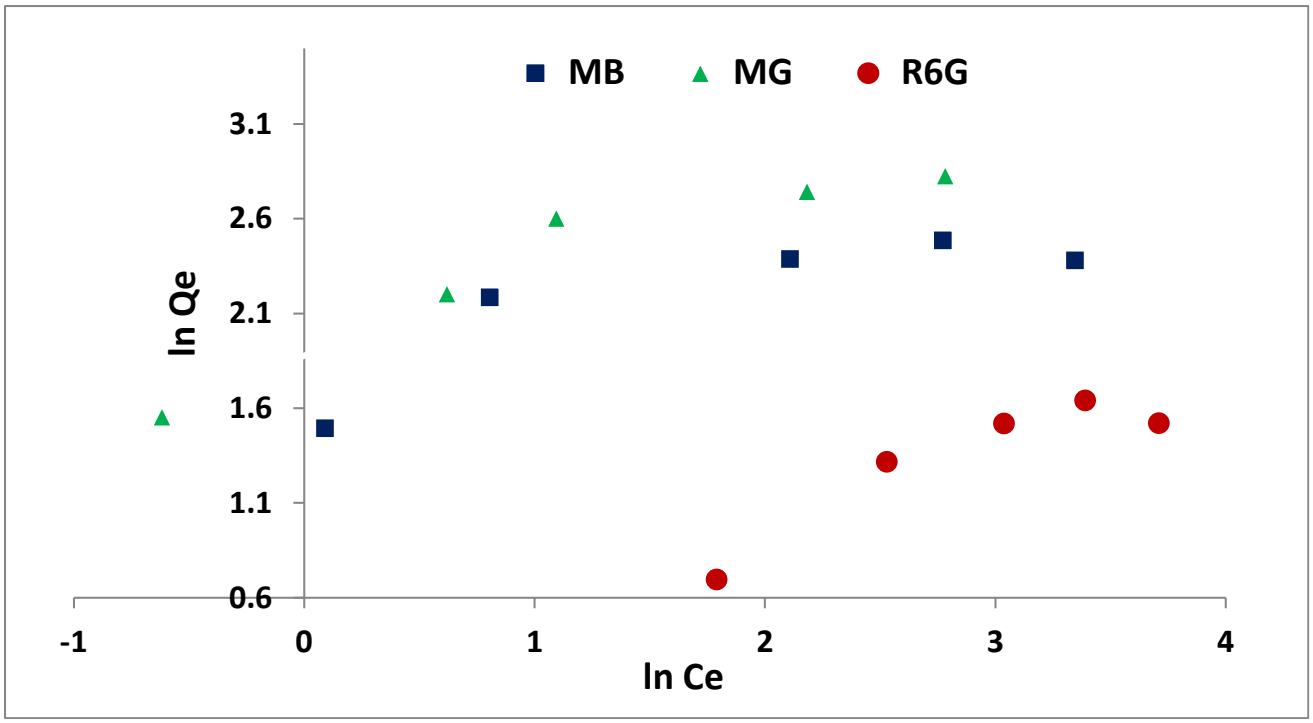

Figure 2.19: Freundlich adsorption isotherm for the removal of 30 mgL^{-1} of MG, 20 mgL^{-1} of MB and R6G at 25 °C pH 7.0

The calculated results of various parameters of the adsorption isotherm models are shown in **Table 2.2**. It can be concluded from the values of correlation coefficient that the dyes follow Langmuir isotherm model. A monolayer adsorption proceeds at certain homogeneous sites on the adsorbent, and all these sites are energetically identical [53]. The results obtained from the adsorption isotherm modelling studies are in agreement with the observations obtained from BET surface area analysis.

Table 2.2: Isotherm constants for the adsorption of 30 mgL^{-1} of MG, 20 mgL^{-1} of MB and R6G at 25 °C pH 7.0

Dye Molecule	Langmuir			Freundlich		
	q_m ($mg\ g^{-1}$)	K_L ($L\ mg^{-1}$)	R^2	N	K_F ($L\ g^{-1}$)	R^2
Malachite Green	18.52	0.0635	0.997	2.69	1.94	0.897
Methylene Blue	11.43	0.0851	0.992	3.99	1.73	0.712
Rhodamine 6G	5.94	1.4237	0.942	2.19	0.02	0.832

2.3.17. Adsorption Kinetics

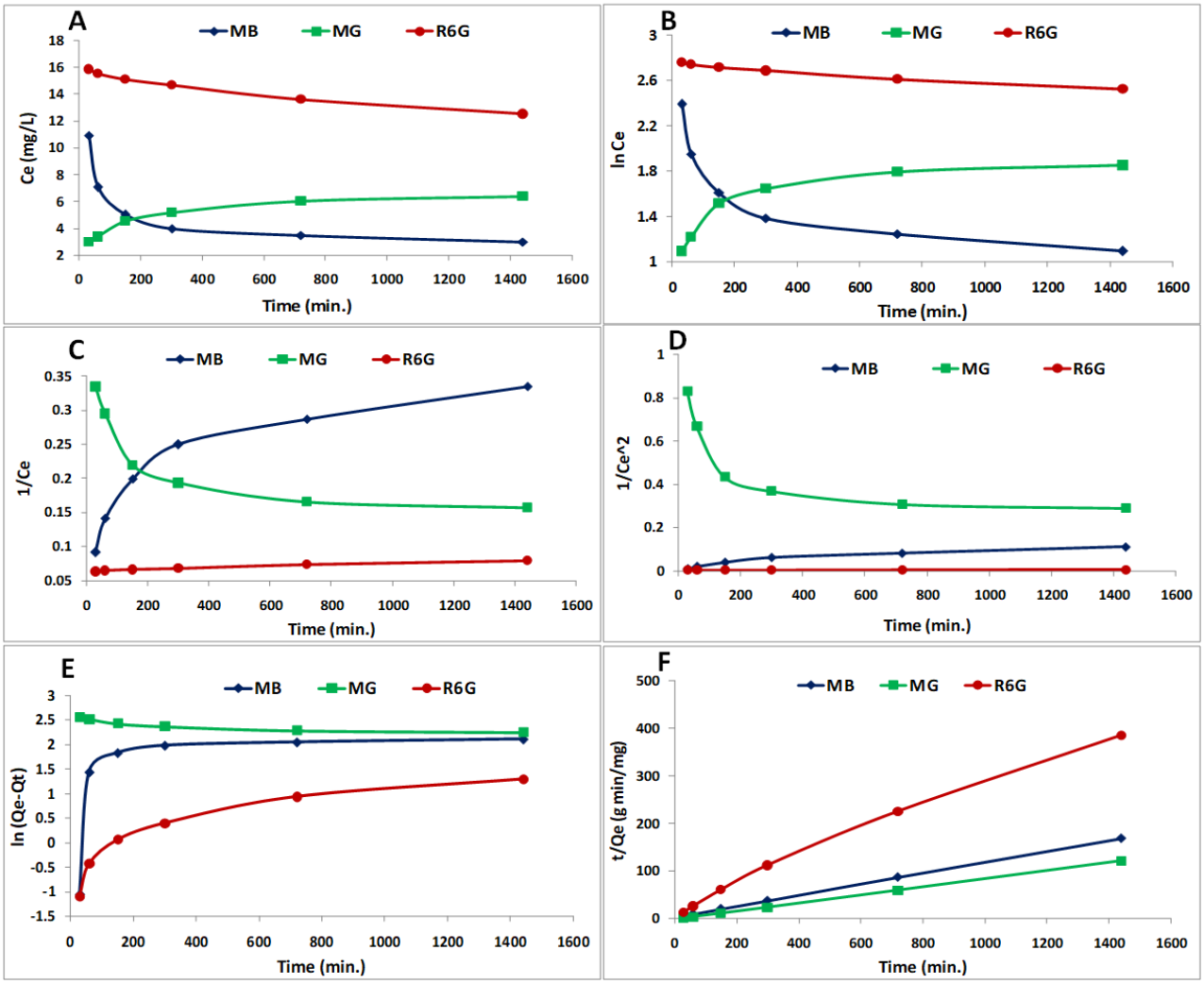

Figure 2.20: (A) Zero order (B) First Order (C) Second Order (D) Third Order (E) Pseudo first order (F) Pseudo Second Order kinetic curves for MB, MG and R6G

Adsorption kinetics validates the linear relationship between the adsorption capacity and time. Several models were employed to ascertain the kinetics of adsorption of the dyes SPNAs. Zero order, First order, second-order, third order, pseudo-first order, pseudo second order models were applied to fit the experimental data. Of all these models pseudo first order and pseudo second order kinetics are studied in detail for establishing the sorption kinetics. The Pseudo first and second order models are expressed as follows[36]

$$ln(q_e - q_t) = ln\, q_e - k_1 t \ldots\ldots\ldots\ldots\ldots (6)$$

$$\frac{t}{q_t} = \frac{1}{k_{2q_e^2}} + \frac{t}{q_e} \ldots\ldots\ldots\ldots (7)$$

Here, q_e and q_t (mg g^{-1}) are the amount of adsorbed dye at equilibrium and at time t (min) respectively. The pseudo first order rate constant is k_1 and pseudo second order rate constant is expressed as k_2 (mg min g^{-1})..

The values of correlation coefficients (R^2) were introduced to ascertain the suitability in a particular model. From the values of R^2 it was concluded that the adsorption kinetics in case of SPNA follows pseudo second order model for all the three dyes as represented in **Figure 2.20**. Thus it can be said that chemisorption process is the rate determining step in the adsorption of dyes on SPNA. The process of adsorption/desorption process is controlled by the occurrence or absence of chemical interactions of the dye molecules with the adsorbent [54]

2.3.18. Simultaneous Adsorption Studies of Hydrophilic and Hydrophobic Dyes

The results of simultaneous adsorption of MG and R6G show that adsorption capacity of MG is higher than that of R6G. The removal efficiency of MG and R6G was found to be 94.58% and 26.48% respectively. The simultaneous adsorption effect of both the dyes on SPNA was determined by using the ratio of adsorption capacities (*Rq*)

$$Rq = \frac{qb, i}{qm, i} \ldots\ldots\ldots\ldots\ldots (8)$$

where, *qb*, *i* and *qm*, *i* are the uptake of dye *i* in the binary system and mono-component system having same initial concentration, respectively.

For simultaneous adsorption, three probable cases are possible: **i)** if $Rq > 1$, synergism condition, suggesting that adsorption of one dye is accelerated in the presence of another dye; **ii)** if $Rq < 1$, antagonism condition, i.e., the adsorption of one dye is inhibited in the presence of another dye and **iii)** if $Rq = 1$, non-interaction condition, the adsorption of both dyes are independent of each other.

In this case we observe value of *Rq* less than 1 which suggests that it is a case of antagonism. Thus the presence of MG affects the adsorption of R6G and a phenomenon of competitive adsorption is observed between both the dyes. This observation can be explained by two

plausible mechanisms i) Out of the various chemical interactions formed between the dyes and SPNA, MG forms hydrogen bonding with adsorbent which is a much stronger interaction. However, R6G is unable to form hydrogen bonding with SPNA. ii) Large size of R6G hinders its rapid encapsulation within the cavity as compared to MG. Hence MG predominates in competitive adsorption[55]. Thus, maximum uptake of MG occurs from the mixture of solution due to its stronger affinity with SPNA surface.

2.3.19. Desorption and Recyclability

The reuse of adsorbent is an important index for defining the efficiency of the adsorbent. In order to assess the reusability of the adsorbent successive adsorption/desorption cycles were carried out[56,57]. Results show that the adsorption capacity decreases after five cycles for all the three dyes (**Figure 2.21**).

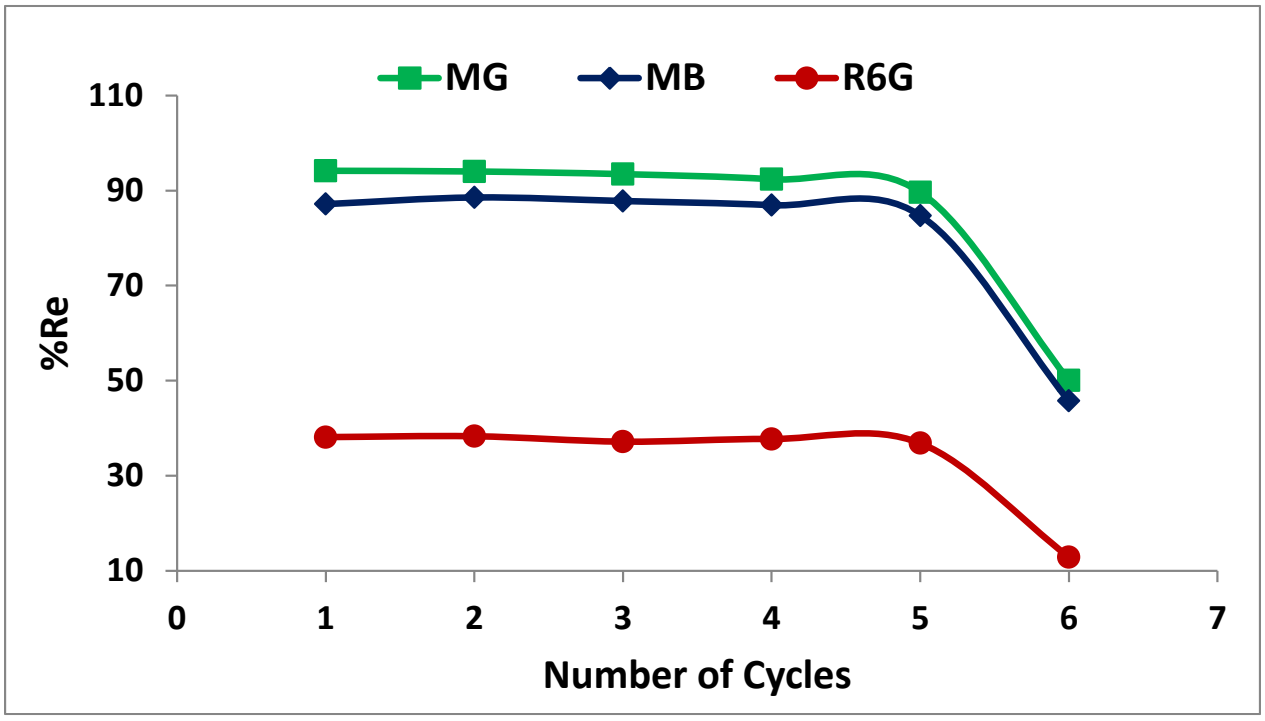

Figure 2.21: Percentage removal of dyes after successive desorption/adsorption cycles

The IR spectra (**Figure 2.22**) and XRD diffractogram (**Figure 2.6**) of the regenerated material shows no significant shifts in the bands or 2θ values. The same characteristics peaks are observed in the IR of the regenerated SPNA as those observed in fresh SPNA. But there is a decrease in the intensities of the IR peaks which may be due to minor degradation caused to

SPNA during the process of desorption. However the degradation doesn't affect the removal efficiency of the material and hence the recycling does not compromise the performance of the adsorbent for dye removal[41]. Similar observations were seen in XRD diffractogram.

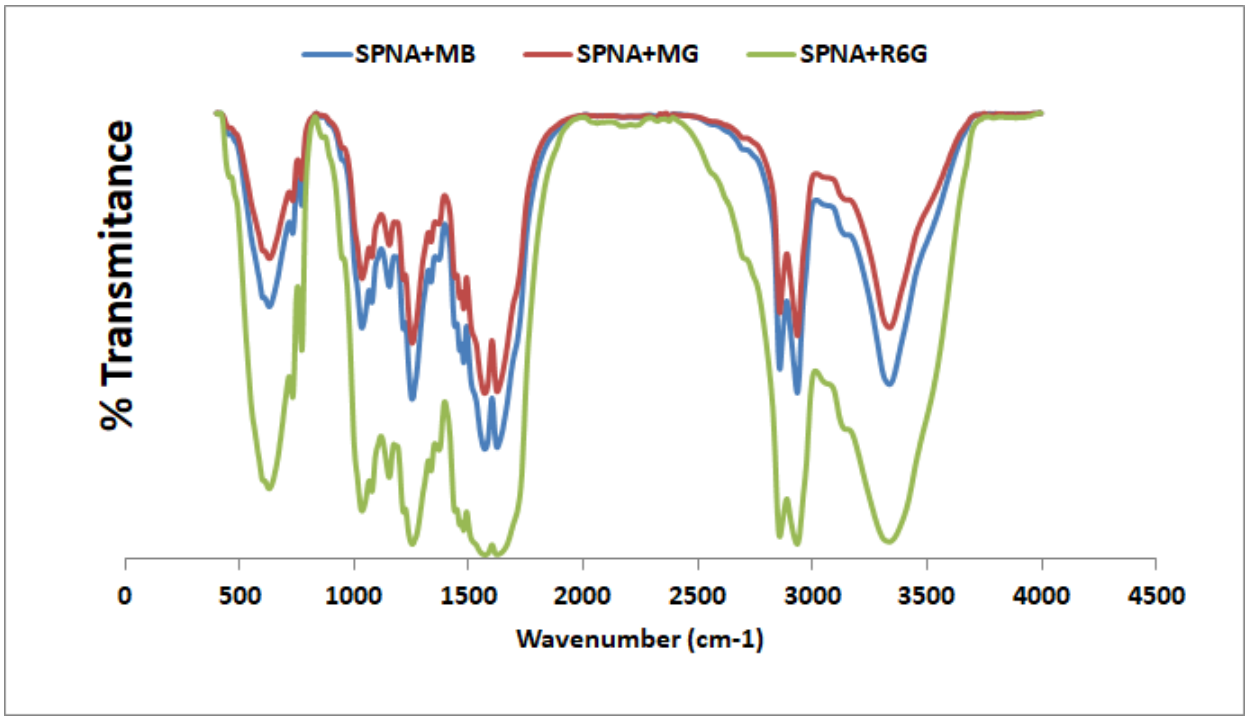

Figure 2.22: FTIR spectra of the recycled adsorbent

2.3.20. Adsorption Mechanism

The probable interaction of SPNA with different dyes is shown in **Figure 2.23**. The mechanism of adsorption is governed by various factors like the structure and functional behavior of adsorbate molecules and surface characteristics of the adsorbent. The adsorbate in this case is dye molecule which is planar and can be readily adsorbed on the adsorbent via van der Waals force and hydrogen bonding interactions in addition to CD cavity. Further, in case of cationic dyes the electrostatic forces of interaction play a role in the sorption process.

The cavity of cyclodextrin can encapsulate all the three types of organic dyes[10]. But lower adsorption of R6G suggests that its larger size and hydrophobic nature prevent any other interaction with the SPNA. On the other hand MB and MG are able to bind to the CD-MA polymer via electrostatic forces of interaction, van der Waals forces and hydrogen bonding in addition to the host guest interaction with the cavity of cyclodextrin.

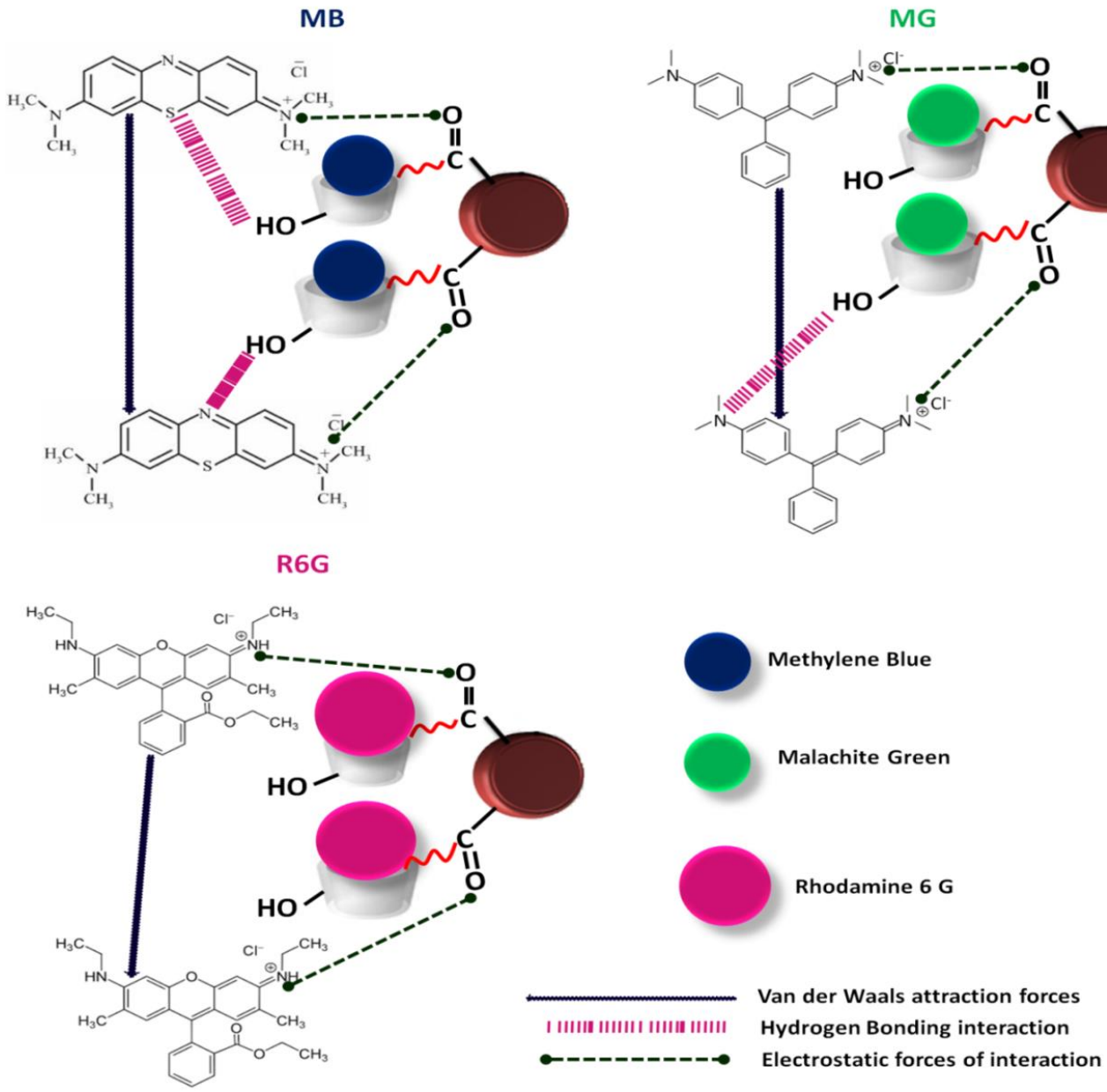

Figure 2.23: Interaction of the dyes MB, MG and R6G with SPNA

The elemental composition of the adsorbent prior to and after, adsorption/desorption cycles can be used to compare the characteristic changes of dye loaded adsorbents (**Table 2.3**).The higher content of carbon after adsorption suggests the successful adsorption of the dyes on the surface of SPNA. The presence of elements like nitrogen, and sulphur on adsorbent + MG, adsorbent + MG and adsorbent + R6G further prove their presence on the adsorbent by virtue of adsorption.

Thus it can be assumed that the changes in the composition of elements correspond to adsorption of the dyes which may be due to these possible interactions.

Table 2.3: Elemental composition of adsorbent determined before and after adsorption following 4 adsorption/desorption cycles

Materials	C (Weight %)	Fe (Weight %)	O (Weight %)	N (Weight %)	S (Weight %)
Bare adsorbent	30.39	7.05	62.57	0	0
Adsorbent +MG	46.75	6.76	31.92	14.75	0
Adsorbent+R6G	40.28	22.58	31.27	5.86	0
Adsorbent +MB	36.71	34.46	23.29	5.41	0.12

2.3.21. Comparison with Other Adsorbents

Table 2.4: Comparison of maximum adsorption capacities of SPNA with other adsorbents

ADSORBENT	ADSORBATE	Q_m (mg/g)	Reference
ZnO particles	MG	13.6	[58]
rGO	MG	13.52	[59]
SPNA	MG	18.52	This work
EDTA-β-CD	MB	0.262	[41]
C. racemosa var. Cylindracea	MB	5.23	[60]
CAS	MB	8.52	[61]
SPNA	MB	11.43	This work
Trichoderma harzianum mycelial waste	R6G	3.40	[62]
Na^+-Montmorillonite	R6G	0.40	[63]
SPNA	R6G	5.94	This work

The values of maximum adsorption capacities of the dyes on SPNA obtained from experiments have been compared with other results reported in literature (**Table 2.4**). It is observed that SPNA has a greater adsorption capability as compared to other adsorbents. The results prove that

the SPNA can be considered as a promising adsorbent for dye removal especially Malachite Green. The literature values also reveal the lower adsorption efficiency in case of R6G probably due to its larger size.

2.4.Conclusion

In summary, this work has established a proficient and simple approach to prepare a novel magnetic nano-adsorbent (SPNA) which can efficiently remove organic dyes particularly MB, MG and R6G. The results indicate that SPNA is an excellent nano-adsorbent for removal of dyes with maximum removal efficiency of 97.2%, 85.1% and 37.3% for MB, MG and R6G, respectively. The main advantage of maleic anhydride cross-linked cyclodextrin polymer is that it facilitates simultaneous adsorption of hydrophobic as well as hydrophilic dyes. The detailed investigation of adsorption behavior of the SPNA exhibited that adsorption process was dominated by the Van der Waal interactions between the SPNA and dye molecules. The removal efficiency is regulated by concentration, adsorbent dose, pH and temperature. The adsorption kinetic studies reveal that removal of organic dye is spontaneous process and obeys the pseudo second order model. The equilibrium data were best fitted with Langmuir isotherm model. Furthermore, SPNA can be regenerated and reused for five cycles with slight decrease in removal efficiency and can be easily separated by magnetic decantation. Thus, convenient, highly efficient and technically feasible properties make this novel nano-adsorbent a promising low cost adsorbent for dye removal. It can be concluded from the results that this superparamagnetic nano-adsorbent can be used for environmental remediation effectively.

References

(1) Qian, Y.; Yuan, Y.; Wang, H.; Liu, H.; Zhang, J.; Shi, S.; Guo, Z.; Wang, N. Highly Efficient Uranium Adsorption by Salicylaldoxime/Polydopamine Graphene Oxide Nanocomposites. *J. Mater. Chem. A* 2018, *6* (48), 24676–24685. https://doi.org/10.1039/C8TA09486A.

(2) Zhang, H.; Lyu, S.; Zhou, X.; Gu, H.; Ma, C.; Wang, C.; Ding, T.; Shao, Q.; Liu, H.; Guo, Z. Super Light 3D Hierarchical Nanocellulose Aerogel Foam with Superior Oil Adsorption. *J. Colloid Interface Sci.* 2019, *536*, 245–251. https://doi.org/10.1016/j.jcis.2018.10.038.

(3) Hu, Q.; Zhou, N.; Gong, K.; Liu, H.; Liu, Q.; Sun, D.; Wang, Q.; Shao, Q.; Liu, H.; Qiu, B.; et al. Intracellular Polymer Substances Induced Conductive Polyaniline for Improved Methane Production from Anaerobic Wastewater Treatment. *ACS Sustain. Chem. Eng.* 2019, *7*, 5912–5920. https://doi.org/10.1021/acssuschemeng.8b05847.

(4) Mehta, D.; Mazumdar, S.; Singh, S. K. Magnetic Adsorbents for the Treatment of Water/Wastewater-A Review. *J. Water Process Eng.* 2015, *7*, 244–265. https://doi.org/10.1016/j.jwpe.2015.07.001.

(5) Qi, W.; Singer, H.; Berg, M.; Müller, B.; Pernet-Coudrier, B.; Liu, H.; Qu, J. Elimination of Polar Micropollutants and Anthropogenic Markers by Wastewater Treatment in Beijing, China. *Chemosphere* 2015, *119*, 1054–1061. https://doi.org/10.1016/j.chemosphere.2014.09.027.

(6) Ling, Y.; Klemes, M. J.; Xiao, L.; Alsbaiee, A.; Dichtel, W. R.; Helbling, D. E. Benchmarking Micropollutant Removal by Activated Carbon and Porous β -Cyclodextrin Polymers under Environmentally Relevant Scenarios. *Environ. Sci. Technol.* 2017, *51* (13), 7590–7598.

(7) Jadeja, R. N.; Tewari, A. Effect of Soda Ash Industry Effluent on Bioaccumulation of Metals by Seaweeds of Coastal Region of Gujarat , India. *J. Hazard. Mater.* 2007, *147*, 148–154. https://doi.org/10.1016/j.jhazmat.2006.12.060.

(8) Jadeja, R. N.; Tewari, A. Effect of Soda Ash Industry Effluent on Protein Content of Two

Green Seaweeds. *J. Hazard. Mater.* 2008, *151*, 559–561. https://doi.org/10.1016/j.jhazmat.2007.06.015.

(9) Jadeja, R. N.; Tewari, A. Effect of Soda Ash Industry Effluent on Agarophytes , Alginophytes and Carrageenophyte of West Coast of India. *J. Hazard. Mater.* 2009, *162*, 498–502. https://doi.org/10.1016/j.jhazmat.2008.05.080.

(10) Ebadi, A.; Rafati, A. A. Preparation of Silica Mesoporous Nanoparticles Functionalized with β-Cyclodextrin and Its Application for Methylene Blue Removal. *J. Mol. Liq.* 2015, *209* (1), 239–245. https://doi.org/10.1016/j.molliq.2015.06.009.

(11) Sharma, Y. C. Optimization of Parameters for Adsorption of Methylene Blue on a Low-Cost Activated Carbon. *J. Chem. Eng. Data* 2010, *55*, 435–439.

(12) Sharma, Y. C. Adsorption Characteristics of a Low-Cost Activated Carbon for the Reclamation of Colored Effluents Containing Malachite Green. *J. Chem. Eng. Data* 2011, *56*, 478–484.

(13) Agarwal, S.; Tyagi, I.; Gupta, V. K.; Mashhadi, S.; Ghasemi, M. Kinetics and Thermodynamics of Malachite Green Dye Removal from Aqueous Phase Using Iron Nanoparticles Loaded on Ash. *J. Mol. Liq.* 2016, *223*, 1340–1347. https://doi.org/10.1016/j.molliq.2016.04.039.

(14) Haroon, M.; Wang, L.; Yu, H.; Summe, R.; Ullah, R.; Chen, Q.; Liu, J. Synthesis of Carboxymethyl Starch- g -Polyvinylpyrolidones and Their Properties for the Adsorption of Rhodamine 6G and Ammonia. *Carbohydr. Polym.* 2018, *186*, 150–158. https://doi.org/10.1016/j.carbpol.2018.01.052.

(15) Liu, L.; Gao, Z. Y.; Su, X. P.; Chen, X.; Jiang, L.; Yao, J. M. Adsorption Removal of Dyes from Single and Binary Solutions Using a Cellulose-Based Bioadsorbent. *ACS Sustain. Chem. Eng.* 2015, *3* (3), 432–442. https://doi.org/10.1021/sc500848m.

(16) Nekouei, F.; Nekouei, S.; Tyagi, I.; Gupta, V. K. Kinetic, Thermodynamic and Isotherm Studies for Acid Blue 129 Removal from Liquids Using Copper Oxide Nanoparticle-Modified Activated Carbon as a Novel Adsorbent. *J. Mol. Liq.* 2015, *201*, 124–133.

https://doi.org/10.1016/j.molliq.2014.09.027.

(17) Yang, S. T.; Chen, S.; Chang, Y.; Cao, A.; Liu, Y.; Wang, H. Removal of Methylene Blue from Aqueous Solution by Graphene Oxide. *J. Colloid Interface Sci.* 2011, *359* (1), 24–29. https://doi.org/10.1016/j.jcis.2011.02.064.

(18) Karthikeyan, K. T.; Nithya, A.; Jothivenkatachalam, K. Photocatalytic and Antimicrobial Activities of Chitosan-TiO2 Nanocomposite. *Int. J. Biol. Macromol.* 2017, *104*, 1762–1773. https://doi.org/10.1016/j.ijbiomac.2017.03.121.

(19) Wu, X.; Hui, K. N.; Hui, K. S.; Lee, S. K.; Zhou, W.; Chen, R.; Hwang, D. H.; Cho, Y. R.; Son, Y. G. Adsorption of Basic Yellow 87 from Aqueous Solution onto Two Different Mesoporous Adsorbents. *Chem. Eng. J.* 2012, *180*, 91–98. https://doi.org/10.1016/j.cej.2011.11.009.

(20) El-Zahhar, A. A.; Awwad, N. S.; El-Katori, E. E. Removal of Bromophenol Blue Dye from Industrial Waste Water by Synthesizing Polymer-Clay Composite. *J. Mol. Liq.* 2014, *199*, 454–461. https://doi.org/10.1016/j.molliq.2014.07.034.

(21) Hong, Y.; Kim, J.; Choi, A.; Pal, M.; Lee, G. RSC Advances Highly Stable Mesoporous Silica Nanospheres Embedded with FeCo / Graphitic Shell Nanocrystals as Magnetically Recyclable Multifunctional Adsorbents for Wastewater Treatment †. *RSC Adv.* 2017, *8*, 1089–1097. https://doi.org/10.1039/C7RA12240C.

(22) Gupta, V. K.; Agarwal, S.; Saleh, T. A. Synthesis and Characterization of Alumina-Coated Carbon Nanotubes and Their Application for Lead Removal. *J. Hazard. Mater.* 2011, *185* (1), 17–23. https://doi.org/10.1016/j.jhazmat.2010.08.053.

(23) Guleria, A.; Kumari, G.; Lima, E. C. Cellulose-g-Poly-(Acrylamide-Co-Acrylic Acid) Polymeric Bioadsorbent for the Removal of Toxic Inorganic Pollutants from Wastewaters. *Carbohydr. Polym.* 2020, *228*, 115396. https://doi.org/10.1016/j.carbpol.2019.115396.

(24) Mittal, A.; Kaur, D.; Malviya, A.; Mittal, J.; Gupta, V. K. Adsorption Studies on the Removal of Coloring Agent Phenol Red from Wastewater Using Waste Materials as Adsorbents. *J. Colloid Interface Sci.* 2009, *337* (2), 345–354.

https://doi.org/10.1016/j.jcis.2009.05.016.

(25) Valodkar, M.; Singh, P.; Jadeja, R. N.; Thounaojam, M.; Devkar, R.; Thakore, S. Cytotoxicity Evaluation and Antimicrobial Studies of Starch Capped Water Soluble Copper Nanoparticles. *J. Hazard. Mater.* 2012, *202*, 244–249. https://doi.org/10.1016/j.jhazmat.2011.11.077.

(26) Ho, T. A.; Greathouse, A.; Lee, A. S.; Criscenti, L. J. Enhanced Ion Adsorption on Mineral Nanoparticles. *Langmuir* 2018, *34*, 5926–5934. https://doi.org/10.1021/acs.langmuir.8b00680.

(27) Li, X.; Xie, L.; Yang, X.; Nie, X. Adsorption Behavior and Mechanism of β-Cyclodextrin – Styrene-Based Polymer for Cationic Dyes. *RSC Adv.* 2018, *8*, 40321–40329. https://doi.org/10.1039/c8ra07709f.

(28) Brião, G. V.; Jahn, S. L.; Foletto, E. L.; Dotto, G. L. Highly Efficient and Reusable Mesoporous Zeolite Synthetized from a Biopolymer for Cationic Dyes Adsorption. *Colloids Surfaces A Physicochem. Eng. Asp.* 2018, *556*, 43–50. https://doi.org/10.1016/j.colsurfa.2018.08.019.

(29) Hu, X. S.; Liang, R.; Sun, G. Super-Adsorbent Hydrogel for Removal of Methylene Blue Dye from Aqueous Solution. *J. Mater. Chem. A* 2018, *6* (36), 17612–17624. https://doi.org/10.1039/c8ta04722g.

(30) Li, D.; Li, Q.; Bai, N.; Dong, H.; Mao, D. One-Step Synthesis of Cationic Hydrogel for Efficient Dye Adsorption and Its Second Use for Emulsified Oil Separation. *ACS Sustain. Chem. Eng.* 2017, *5* (6), 5598–5607. https://doi.org/10.1021/acssuschemeng.7b01083.

(31) Asfaram, A.; Ghaedi, M.; Hajati, S.; Goudarzi, A. Synthesis of Magnetic γ-Fe2O3-Based Nanomaterial for Ultrasonic Assisted Dyes Adsorption: Modeling and Optimization. *Ultrason. Sonochem.* 2016, *32*, 418–431. https://doi.org/10.1016/j.ultsonch.2016.04.011.

(32) Othman, N. H.; Alias, N. H.; Shahruddin, M. Z.; Abu Bakar, N. F.; Nik Him, N. R.; Lau, W. J. Adsorption Kinetics of Methylene Blue Dyes onto Magnetic Graphene Oxide. *J. Environ. Chem. Eng.* 2018, *6* (2), 2803–2811. https://doi.org/10.1016/j.jece.2018.04.024.

(33) Rathore, P. S.; Patidar, R.; Shripathi, T.; Thakore, S. Magnetically Separable Core–Shell Iron Oxide@nickel Nanoparticles as High-Performance Recyclable Catalysts for Chemoselective Reduction of Nitroaromatics. *Catal. Sci. Technol.* 2015, *5*, 286–295. https://doi.org/10.1039/C4CY00673A.

(34) Wu, N.; Liu, C.; Xu, D.; Liu, J.; Liu, W.; Shao, Q.; Guo, Z. Enhanced Electromagnetic Wave Absorption of Three-Dimensional Porous Fe 3 O 4 /C Composite Flowers. *ACS Sustain. Chem. Eng.* 2018, *6* (9), 12471–12480. https://doi.org/10.1021/acssuschemeng.8b03097.

(35) Cai, X.; Liu, Q.; Xia, C.; Shan, D.; Du, J. Recyclable Capture and Destruction of Aqueous Micropollutants Using the Molecule-Specific Cavity of Cyclodextrin Polymer Coupled With. *Environ. Sci. Technol.* 2015, *49* (15), 9264–9272.

(36) Wu, Y.; Qi, H.; Shi, C.; Ma, R.; Liu, S.; Huang, Z. Preparation and Adsorption Behaviors of Sodium Alginate-Based Adsorbent-Immobilized β-Cyclodextrin and Graphene Oxide. *RSC Adv.* 2017, *7*, 31549–31557. https://doi.org/10.1039/C7RA02313H.

(37) Yadav, M.; Das, M.; Thakore, S.; Jadeja, R. N. Surface Modified Magnetic Nanoparticles : A New Generation of Nanoadsorbents for Facile Remediation Protocols. *Environment at Crossroads Challenges and Green Solutions*; 2021; pp 291–311.

(38) Solanki, A.; Sanghvi, S.; Devkar, R.; Thakore, S. β-Cyclodextrin Based Magnetic Nanoconjugates for Targeted Drug Delivery in Cancer Therapy. *RSC Adv.* 2016, *6* (101), 98693–98707. https://doi.org/10.1039/c6ra18030b.

(39) Zhang, J.; Li, Y.; Bao, M.; Yang, X.; Wang, Z.; Zhang, J.; Li, Y.; Bao, M.; Yang, X.; Wang, Z. Facile Fabrication of Cyclodextrin-Modified Magnetic Particles for Effective Demulsification from Various Types of Emulsions Facile Fabrication of Cyclodextrin-Modified Magnetic Particles for Effective Demulsification from Various Types of Emulsions. *Environ. Sci. Technol.* 2016, *50* (16), 8809–8816. https://doi.org/10.1021/acs.est.6b01941.

(40) Das, M.; Solanki, A.; Joshi, A.; Devkar, R.; Seshadri, S. β -Cyclodextrin Based Dual-Responsive Multifunctional Nanotheranostics for Cancer Cell Targeting and Dual Drug

Delivery. *Carbohydr. Polym.* 2019, *206*, 694–705. https://doi.org/10.1016/j.carbpol.2018.11.049.

(41) Zhao, F.; Repo, E.; Yin, D.; Meng, Y.; Jafari, S.; Sillanpaa, M. EDTA-Cross-Linked β-Cyclodextrin : An Environmentally Friendly Bifunctional Adsorbent for Simultaneous Adsorption of Metals and Cationic. *Environ. Sci. Technol.* 2015, *49* (17), 10570–10580.

(42) Wang, D.; Liu, L.; Jiang, X.; Yu, J.; Chen, X. Adsorption and Removal of Malachite Green from Aqueous Solution Using Magnetic β-Cyclodextrin-Graphene Oxide Nanocomposites as Adsorbents. *Colloids Surfaces A Physicochem. Eng. Asp.* 2015, *466*, 166–173. https://doi.org/10.1016/j.colsurfa.2014.11.021.

(43) Girek, T.; Shin, D. H.; Lim, S. T. Polymerization of β-Cyclodextrin with Maleic Anhydride and Structural Characterization of the Polymers. *Carbohydr. Polym.* 2000, *42* (1), 59–63. https://doi.org/10.1016/S0144-8617(99)00138-1.

(44) Park, J. O.; Rhee, K. Y.; Park, S. J. Silane Treatment of Fe 3 O 4 and Its Effect on the Magnetic and Wear Properties of Fe 3 O 4 /Epoxy Nanocomposites. *Appl. Surf. Sci.* 2010, *256* (23), 6945–6950. https://doi.org/10.1016/j.apsusc.2010.04.110.

(45) Solanki, A.; Thakore, S. Cellulose Crosslinked PH-Responsive Polyurethanes for Drug Delivery: α-Hydroxy Acids as Drug Release Modifiers. *Int. J. Biol. Macromol.* 2015, *80*, 683–691. https://doi.org/10.1016/j.ijbiomac.2015.07.003.

(46) Solanki, A. R.; Kamath, B. V.; Thakore, S. Carbohydrate Crosslinked Biocompatible Polyurethanes: Synthesis, Characterization, and Drug Delivery Studies. *J. Appl. Polym. Sci.* 2015, *132* (28), 42223. https://doi.org/10.1002/app.42223.

(47) Meier, M. M.; Luiz, M. T. B.; Szpoganicz, B.; Soldi, V. Thermal Analysis Behavior of β- and γ-Cyclodextrin Inclusion Complexes with Capric and Caprilic Acid. *Thermochim. Acta* 2001, *375*, 153–160.

(48) Chen, J.; He, F.; Zhang, H.; Zhang, X.; Zhang, G.; Yuan, G. Novel Core-Shell Structured Mn-Fe/MnO2magnetic Nanoparticles for Enhanced Pb(II) Removal from Aqueous Solution. *Ind. Eng. Chem. Res.* 2014, *53* (48), 18481–18488.

https://doi.org/10.1021/ie502967a.

(49) Brown, T. C.; Miron, D. J.; Fellows, C. M. Pressure-Varying Langmuir Parameters and Stepped Nitrogen Adsorption on Alumina and Silica. *Phys. Chem. Chem. Phys.* 2019, *21* (5), 2558–2566. https://doi.org/10.1039/c8cp06163g.

(50) Liu, L.; Gao, Z.; Su, X.; Chen, X.; Jiang, L.; Yao, J. Adsorption Removal of Dyes from Single and Binary Solutions Using a Cellulose-Based Bioadsorbent. *ACS Sustain. Chem. Eng.* 2015, *3* (3), 432–442. https://doi.org/10.1021/sc500848m.

(51) Zhou, Y.; Zhang, M.; Hu, X.; Wang, X.; Niu, J.; Ma, T. Adsorption of Cationic Dyes on a Cellulose-Based Multicarboxyl Adsorbent. *J. Chem. Eng. Data* 2013, *58* (2), 413–421. https://doi.org/10.1021/je301140c.

(52) Jalil, A. A.; Triwahyono, S.; Yaakob, M. R.; Azmi, Z. Z. A.; Sapawe, N.; Kamarudin, N. H. N.; Setiabudi, H. D.; Jaafar, N. F.; Sidik, S. M.; Adam, S. H.; et al. Utilization of Bivalve Shell-Treated Zea Mays L. (Maize) Husk Leaf as a Low-Cost Biosorbent for Enhanced Adsorption of Malachite Green. *Bioresour. Technol.* 2012, *120*, 218–224. https://doi.org/10.1016/j.biortech.2012.06.066.

(53) Maruthapandi, M.; Kumar, V. B.; Luong, J. H. T.; Gedanken, A. Kinetics , Isotherm , and Thermodynamic Studies of Methylene Blue Adsorption on Polyaniline and Polypyrrole Macro − Nanoparticles Synthesized by C - Dot-Initiated Polymerization. *ACS Omega* 2018, *3*, 7196–7203. https://doi.org/10.1021/acsomega.8b00478.

(54) Cui, L.; Hu, L.; Du, B.; Gao, L.; Wang, Y.; Wei, Q. Removal of Hg(II) from Aqueous Solution by Resin Loaded Magnetic β-Cyclodextrin Bead and Graphene Oxide Sheet: Synthesis, Adsorption Mechanism and Separation Properties. *J. Colloid Interface Sci.* 2015, *456*, 42–49. https://doi.org/10.1016/j.jcis.2015.06.007.

(55) Ren, H.; Kulkarni, D. D.; Kodiyath, R.; Xu, W.; Choi, I. Competitive Adsorption of Dopamine and Rhodamine 6G on the Surface of Graphene Oxide. *Appl. Mater. Interfaces* 2014, *6*, 2459–2470.

(56) Feng, N.; Guo, X.; Liang, S.; Zhu, Y.; Liu, J. Biosorption of Heavy Metals from Aqueous

Solutions by Chemically Modified Orange Peel. *J. Hazard. Mater.* 2011, *185* (1), 49–54. https://doi.org/10.1016/j.jhazmat.2010.08.114.

(57) Yu, J. X.; Chi, R. A.; Guo, J.; Zhang, Y. F.; Xu, Z. G.; Xiao, C. Q. Desorption and Photodegradation of Methylene Blue from Modified Sugarcane Bagasse Surface by Acid TiO2hydrosol. *Appl. Surf. Sci.* 2012, *258* (8), 4085–4090. https://doi.org/10.1016/j.apsusc.2011.12.106.

(58) Taylor, P.; Husaain, D.; Najam-ul-haq, M.; Saeed, A.; Jabeen, F.; Ashiq, M. N.; Husaain, D.; Najam-ul-haq, M.; Saeed, A.; Jabeen, F.; et al. Treatment Synthesis of Poly GMA / DVB and Its Application for the Removal of Malachite Green from Aqueous Medium by Adsorption Process. *Desalin. Water Treat.* 2013, *53*, 2518–2528. https://doi.org/10.1080/19443994.2013.867538.

(59) Robati, D.; Rajabi, M.; Moradi, O.; Naja, F.; Tyagi, I.; Agarwal, S.; Kumar, V. Kinetics and Thermodynamics of Malachite Green Dye Adsorption from Aqueous Solutions on Graphene Oxide and Reduced Graphene Oxide. *J. Mol. Liq.* 2016, *214*, 259–263. https://doi.org/10.1016/j.molliq.2015.12.073.

(60) Cengiz, S.; Cavas, L. Removal of Methylene Blue by Invasive Marine Seaweed : Caulerpa Racemosa Var . Cylindracea. 2008, *99*, 2357–2363. https://doi.org/10.1016/j.biortech.2007.05.011.

(61) Santhi, T. A New Alternative Adsorbent for the Removal of Cationic Dyes from Aqueous Solution. *Arab. J. Chem.* 2016, *9*, S466–S474. https://doi.org/10.1016/j.arabjc.2011.06.004.

(62) Sadhasivam, S. Ã.; Savitha, S.; Swaminathan, K. Exploitation of Trichoderma Harzianum Mycelial Waste for the Removal of Rhodamine 6G from Aqueous Solution. 2007, *85*, 155–161. https://doi.org/10.1016/j.jenvman.2006.08.010.

(63) Gemeay, A. H. Adsorption Characteristics and the Kinetics of the Cation Exchange of Rhodamine-6G with Na^{+}-Montmorillonite. 2002, *241*, 235–241. https://doi.org/10.1006/jcis.2002.8410.

Paper Published from this Chapter:

ACS OMEGA

Article

Cite This: ACS Omega 2019, 4, 11993−12003

http://pubs.acs.org/journal/acsodf

Maleic Anhydride Cross-Linked β-Cyclodextrin-Conjugated Magnetic Nanoadsorbent: An Ecofriendly Approach for Simultaneous Adsorption of Hydrophilic and Hydrophobic Dyes

Monika Yadav,[†] Manita Das,[‡] Chirag Savani,[‡] Sonal Thakore,*[,‡] and Rajendrasinh Jadeja*[,†,‡]

[†]Department of Environmental Studies, Faculty of Science, and [‡]Department of Chemistry, Faculty of Science, The Maharaja Sayajirao University of Baroda, Vadodara 390 002, India

Supporting Information

ABSTRACT: A magnetic nanoadsorbent with a cross-linked β-Cyclodextrin maleic anhydride polymer capable of simultaneous removal of hydrophilic and hydrophobic dyes was developed with high efficacy and desorption/recycling efficiency. The effect of various parameters (concentration, adsorbent dosage, contact time, pH, and temperature) was evaluated to assess the optimum adsorption conditions. The superparamagnetic nanoadsorbent (SPNA) could be easily separated by magnetic decantation and showed maximum removal of malachite green with 97.2% adsorption efficiency. Studies on simultaneous adsorption of dyes from a mixture were performed and the adsorption capacity was calculated. Interestingly, the phenomenon of competitive adsorption was observed. The adsorption process can be fitted well into the Langmuir isotherm model and follows pseudo-second-order kinetics. SPNA could be effectively regenerated and recycled at least five times without any significant loss in removal efficiency. SPNA could be an ideal adsorbent for water remediation because of excellent dye removal efficiency in addition to chemical stability, ease of synthesis, and better reusability.

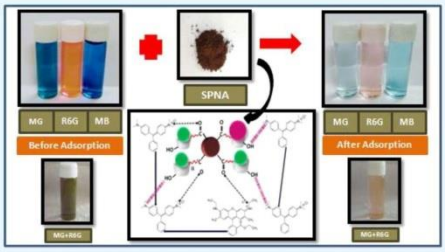

1. INTRODUCTION

In the modern era of industrial development, environmental problems have drawn more and more attention all over the world. Discharge of chemical industries such as textiles, paper, color photography, printing, dye, and food industries that comprise large amounts of contaminants such as dyes and paints pose a risk to agriculture and the food chain and consequently to human health. Independent of the source, a large number of nondegradable pollutants are being discharged in the ecosystem, especially water.[1−5] Synthetic dyes generally have complex aromatic molecular structures and are more resistant toward biodegradation and oxidizing agents. Addition of such less ecofriendly dyes into aquatic systems can lead to several disadvantages and hazards such as hindrance of light penetration as well as mutagenic changes. This in turn leads to increase in chemical oxygen demand and biological oxygen demand of water system.[6−8] Therefore, treatment of dye wastewater prior to discharge into water resources of the environment is a critical task.[9]

Methylene blue (MB), malachite green (MG), and rhodamine are dyes with commercial significance and widely used for dyeing textile fibers like cotton, wool, and so forth. These dyes are also used as analytical reagents. MB is also used in temporary hair coloring. Although not strongly hazardous, it still has various adverse effects on being consumed.[10] MG is a common cationic dye belonging to the triphenylmethane and it is an important indestructible dye. Along with being carcinogenic, the detrimental impact of MG includes excess sweating, eye burn, and so forth.[11] Rhodamine is a relatively hydrophobic dye widely used as a colorant for textiles and food stuffs. Various physical chemical and biological methods have been manifested to eliminate dyes from wastewater. These include adsorption, ozonation, ion exchange, membrane and oxidative processes, and several others. Adsorption technique stands out as a convenient and cost-effective technique to remove dyes and for effluent treatment, among all the demonstrated methods.[12] Till date, numerous adsorbents have been developed in order to remove dyes from aqueous solutions. Some examples are activated carbon,[13] MCM-41 and MCA,[14] graphene oxide,[15] mesoporous SiO_2,[16] polymer-clay,[17] alumina,[18] agricultural wastes,[19] bioadsorbents, nanoadsorbents,[20−22] hydrogels,[23,24] and aerogels.[25,26] Because of a higher surface area, and ability of surface modification, nanoadsorbents exhibit greater efficiency and higher removal rate of pollutants from wastewater.[21,27] Magnetic nanoparticles (MNPs) such as Fe_3O_4 are beneficial for environmental applications because of the rapid dissociation of target

Received: March 30, 2019
Accepted: June 19, 2019
Published: July 10, 2019

DOI: 10.1021/acsomega.9b00881
ACS Omega 2019, 4, 11993−12003